ENGINEERING RESEARCH INSTITUTE
UNIVERSITY OF MICHIGAN
ANN ARBOR

FINAL REPORT

WING-BODY INTERFERENCE

PART II. EXPERIMENTAL INVESTIGATION OF CYLINDRICAL MODEL

By

H. E. BAILEY

R. E. PHINNEY

Projects M937 and M937-1

WRIGHT AIR DEVELOPMENT CENTER, U.S. AIR FORCE
CONTRACT AF 33(038)-19747, E.O. NO. 460-31-12-11 SR-1g

February, 1954

TABLE OF CONTENTS

LIST OF FIGURES

LIST OF FIGURES (cont.)

FINAL REPORT

WING-BODY INTERFERENCE

PART II. EXPERIMENTAL INVESTIGATION

A. INTRODUCTION

This report, which is the second of three parts, presents the experimental results obtained from one of the models tested on Contract AF 33(038)-19747. The experimental results are compared to the theoretical results of reference1 as well as to the theoretical results which were presented in the first part of this final report.

B. SOME EFFECTS OF VISCOSITY IN SUPERSONIC FLOWS

1. General Viscous Effects

Before proceeding with the discussion of the specific results obtained for the configurations tested, it would be well to review what is known about viscous-compressible flows in some of the simpler cases. In general the effect of shock-wave - boundary-layer interaction is twofold: (1) The presence of subsonic velocities in the boundary layer will permit the upstream propagation of pressure disturbances; i.e., the effect of the boundary layer is to provide a channel through which a disturbance in the supersonic flow can influence the flow field upstream of the Mach cone whose apex is at the disturbance. (2) The sharp pressure gradients which may be sustained in a supersonic flow can disturb the boundary layer flow; e.g., even a very weak shock wave impinging on a laminar boundary layer will cause a local separation and consequent transition to turbulent flow in the boundary layer.

2. Effect of Viscosity on Supersonic Flow over Two-Dimensional Wings

One of the simplest possible viscous-compressible flows is the supersonic viscous flow over a wing profile. If the wing is inclined at a positive angle of attack, the nonviscous theory indicates that a Prandtl-Meyer expansion wave will occur at the leading edge. However, it has been observed experimentally in reference 2 that a very weak shock wave precedes the expansion. This weak compression wave is probably a continuation of the fairly strong shock wave which occurs at the leading edge on the lower compression side of the wing and is locally detached at the wing leading edge due to the finite thickness of the leading edge.

On the expansion side of the wing a trailing-edge shock wave must occur which turns the flow approximately back into the free-stream direction. It has been observed[3] that the presence of this shock wave causes the laminar boundary layer to separate from the wing surface as much as 100 boundary-layer thicknesses upstream of the trailing edge. The separated air will tend to cling to the wing surface but it will be accelerated on its periphery by mixing with the free stream. The separated air thus forms a slow subsonic pocket in which the pressure assumes values between the theoretical pressure and the ambient pressure. The overall effect of this separated pocket of air is to reduce both the lift and the drag of the wing.

3. Shock Wave Reflecting from a Boundary Layer

The problem of a shock wave reflecting from the boundary layer on a flat plate has been extensively studied both experimentally[4,5,6] and theoretically[7,8]. Even for weak shock waves, e.g., deflection angles of 2 to 3°, the laminar boundary layer tends to separate approximately 50 to 100 boundary-layer thicknesses upstream of the point of incidence and reattach not far downstream from the point of incidence. This upstream propagation tends to smooth the otherwise sharp pressure rise. If the boundary layer ahead of the point of incidence is turbulent, it is better able to sustain large pressure jumps and will separate locally for only much stronger shock waves[6]. In this case the upstream propagation of the disturbance is confined to a distance of about 10 boundary-layer thicknesses upstream of the point of impingement.

4. Nonreflecting or Grazing Shock - Boundary-Layer Interaction

A grazing shock - boundary-layer interaction may occur on a flat plate which is aligned with the free stream but abuts the root section of a flat-plate wing at angle of attack. In this case there will be no need for a reflected wave; thus the effect of the incident wave will not be increased by the

requirement that a reflected wave originate at the wall. In other words, the pressure gradient which the boundary layer sustains will be approximately one-half what it would be if the wave reflected from the surface. The strength of the wave may vary according to the wing angle of attack, but no matter what the strength of the wave no velocity increment will be induced perpendicular to the end plate. This case differs, however, from the case of a normal shock wave striking a boundary layer, not only in that the strength of the wave may be varied, but also in that there will always be a component of the velocity parallel to the shock wave which will pass through the wave unchanged. It is this parallel component of the velocity which will induce crossflow in the boundary layer. Numerous examples of this grazing type of interaction have been observed with the china-clay film technique; e.g., a tunnel shock wave which intersects the wing plane normal to the wing plane but inclined at approximately the Mach angle with respect to the flow direction (Fig. 7); or the flow in the juncture of a wing-body configuration close enough to the juncture line so that the curvature of the body may be neglected (Fig. 7). In all cases the streamline pattern indicated by the china-clay film shows that the low-inertia air near the surface is deflected through a larger angle than the corresponding outer potential flow. As a matter of fact, if the shock wave is sufficiently strong, the flow may even separate slightly ahead of the shock wave and then reattach downstream, thus forming a separated channel along the foot of the shock wave through which fluid flows out along the shock wave. Specific examples of this type of flow behavior will be mentioned later in the discussions of the various configurations tested.

5. Three-Dimensional Shock-Wave Reflections

If the wing in the example in the previous section abuts a circular body instead of a flat plate, the simplest case of wing-body interaction is obtained. In this case, as the shock wave progresses around the cylinder a velocity will be induced normal to the cylinder. A reflected wave of varying strength will be required to cancel this induced velocity. If the wave from the wing leading edge is a compressive wave, the velocity induced will be away from the cylindrical surface, so that an expansion wave will be required to maintain the flow tangential to the surface, and prevent the flow from separating from the surface.

Another example of three-dimensional shock-wave reflections is the intersection of a plane shock wave and a circular cylinder. This case has been studied theoretically[9,10] as well as experimentally[11]. The flow on the lee side of the cylinder in this case is qualitatively similar to the flow mentioned in the preceding paragraph, i.e., that with a wing mounted on a cylindrical body. The chief difference lies in the fact that if the wing abuts the cylinder the velocity in the wing plane $\theta = 0$ is constant for all values of x, while in the shock cylinder problem the velocity in the plane $\theta = 0$ varies with x.

C. DESCRIPTION OF EXPERIMENTS

1. Applicability of the Experimental Data

While the model which was tested and is described in detail in the next section is not a scale model of any actual airplane or missile, it does contain all the essential features present in wing-body interference configurations. The experimental results presented here are not intended to be applied to any specific configuration, but rather it is hoped that they will lead to a qualitative understanding of the effects of viscosity on wing-body interference problems in general.

The Reynolds number for these tests based on a 2-inch-diameter body is 7×10^5, which corresponds to an actual missile of 2-foot diameter flying at Mach number 1.9 at an altitude of 90,000 feet, or to a missile of 2-inch diameter flying at Mach number 1.9 at an altitude of 37,000 feet. Since the body boundary layer is turbulent, such viscous effects as boundary-layer crossflow and separation are not expected to vary appreciably over a wide range of Reynolds numbers, so that the overall picture obtained from these experimental results is probably valid in general and should indicate the magnitude of the viscous effects fairly accurately.

The agreement between the experimental results and the linearized inviscid theory is sufficiently good to indicate that the effect of Mach number variation on the experimental results will be given fairly well by the Prandtl-Glauert rule, at least for Mach numbers in the range for which the linearized theory is valid.

2. Description of Model

The test results reported here were obtained in the University of Michigan 8- by 13-inch Mach-number-1.9 channel. A complete description of this test facility is contained in reference 12.

The model consists of a cylindrical body and two half-wings. A typical test configuration is illustrated in Fig. 1. The body is hollow with a 2-inch outside diameter and 1-1/2-inch inside diameter. There are two nosepieces which may be used in conjunction with the body. The first nosepiece is 2-9/16 inches long and tapers down to an inlet diameter of 1-5/16 inches. When this nose is used the wing leading edge lies between 2-3/4 inches and 3-3/4 inches aft of the body nose. The second nosepiece is 8-7/16 inches long and tapers at

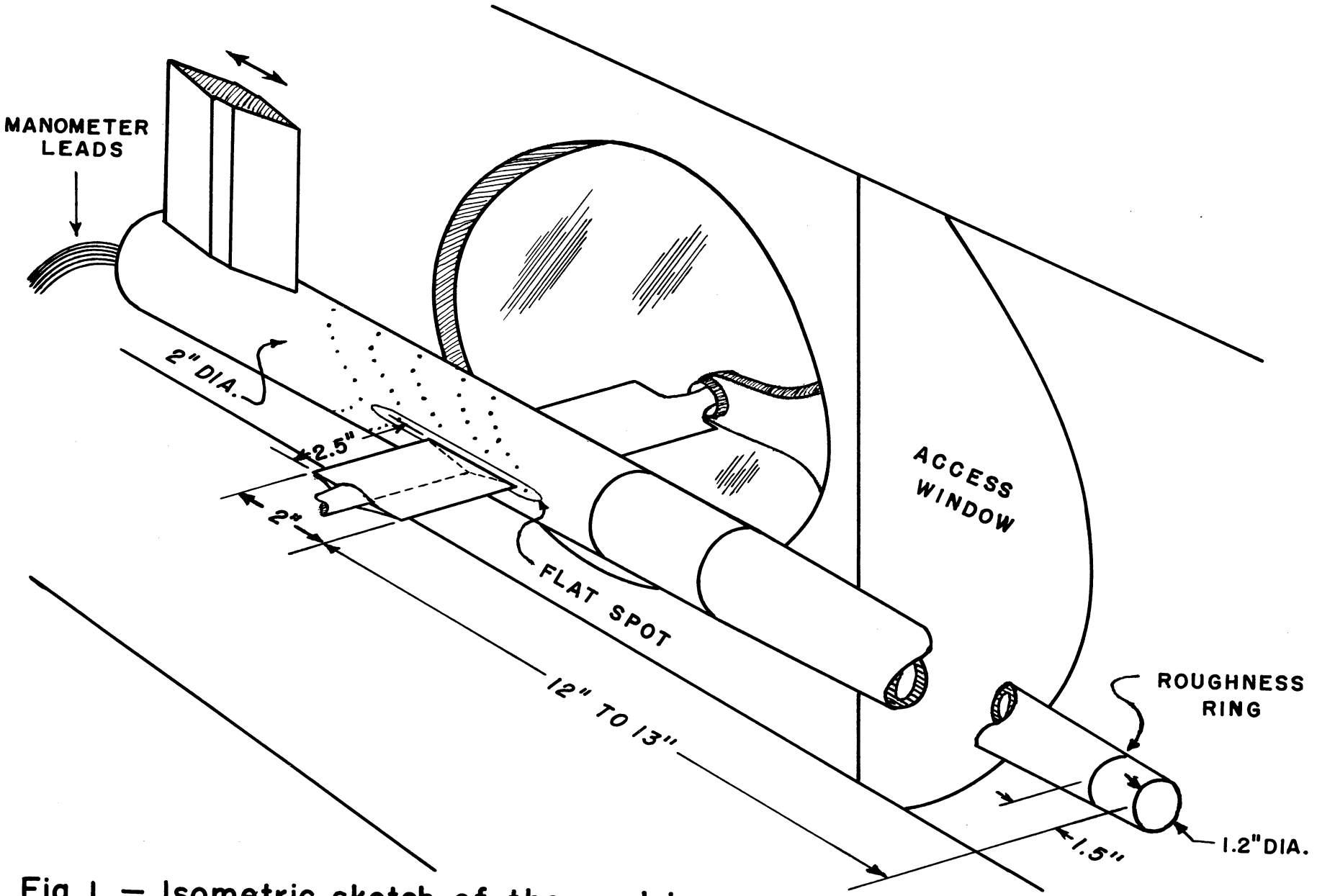

Fig. 1. — Isometric sketch of the model

3-1/2° down to an inlet diameter of 1-1/8 inches. This second nose was always used in conjunction with a 2-1/2-inch long spacer (Fig. 1), so that the distance from the nose of the body to the wing leading edge varied between 12-1/2 inches and 13-1/2 inches. As shown in Fig. 1, a fine 0.016 inch-diameter wire is located 1-1/2 inches from the nose. The purpose of this ring is to insure a stable transition region for the body boundary layer.

The reason for making the body hollow is to produce a nose shock which is as weak as possible and at the same time to keep the model length down to a reasonable value. The reflection of the nose shock from the tunnel sidewalls strikes the body upstream of the orifice region, and the reflection of the nose shock from the tunnel floor and ceiling strikes the body downstream of the orifice region for all body positions. Thus, the orifice region is free of direct body-pressure field effects, and consequently the static pressure is relatively constant in the orifice region for the body alone at zero angle of attack.

The flat spots on the sides of the body (Fig. 1) where the wings abut the body are necessary to prevent a gap between body and wing when the wing is at an angle of incidence with respect to the body. The effects of these flat spots on the body-pressure field are negligible, so far as could be determined from the pressure readings on the body.

It is possible to mount the body at either a 0 or 8° angle of attack with respect to the free stream. Furthermore, with the body at either angle of attack provisions have been made for about 1-1/2 inches of axial motion of the body. The axial position of the body with respect to the wing leading edge was determined for each test position to within $\pm$0.003 inch. Since the wings are fixed with respect to the tunnel, this axial body motion permits the measurement of pressure profiles on the body due to the presence of the wing. The body contains 92 pressure orifices, which lie in planes inclined at angles of 40° with respect to the body axis and 1 inch apart along the axis. The orifices also lie in the meridional planes $\theta = \pm 0, \pm 5, \pm 10, \pm 15, \pm 20, \pm 30, \pm 40, \pm 50, \pm 60, \pm 75$, and $\pm 90°$. Figure 1 does not show the exact position of all the orifices, but it does indicate the extent of the orifice pattern.

The two half-wings, which are supported by brackets outside the tunnel test section, are also shown in Fig. 1. The sealing of the wing-body juncture was effectively accomplished by mechanical contact. There was little leakage between the upper and lower wing surfaces, as indicated by the fact that those orifices which were covered by the wing when the body was moved did not move from their initial position during the run, even though the difference between manometer-tube and tunnel pressures was large. The chord of these wings is 2 inches and the half-span is 2-1/2 inches. The wing cross section is flat on one side, and double-wedge-shaped on the other side with a wedge angle of 10°. The wings may be mounted at angles of attack of 0, $\pm$4, and $\pm$8° with the flat side either up or down. The accuracy of the angle of attack settings is $\pm$0.1°.

3. Instrumentation

All the static pressures were measured with mercury manometers which are photographed during the test run and then reduced later to the ratio of static to stagnation pressure. This technique permits the measurement of static pressures with an accuracy of 1 percent of the ambient pressure.

In addition to the pressure data, at least one schlieren photograph of each configuration was obtained. Unfortunately, the cylindrical body and the wing support bracket obscure the most interesting portion of the schlieren field. However, it is possible to obtain from the pictures a rough idea of the thickness of the body boundary layer in the meridional planes $\theta = \pm 90°$.

The china-clay film technique, which is described in detail in reference 13, was also used on each configuration to illustrate the flow directions in the boundary layer close to the surface of the body and the wing. This technique is especially useful in locating the traces of shock waves on the model surface and in obtaining some idea of the boundary-layer crossflow on the body and wing.

Several attempts to use the vapor-screen technique mentioned in reference 14 failed to give a detailed picture of the flow in the juncture region.

An attempt to obtain a stereoptic pair of schlieren photographs to show the three-dimensional character of the shock waves was not successful.

4. Treatment and Presentation of Experimental Data

All the curves presented for the various configurations are plots of $\beta C_p/\alpha_{B,w}$ vs. x/β, where $\beta = \sqrt{M_\infty^2 - 1}$ and α_w and α_B are the wing and body angles of attack respectively. The zero base for all pressure curves is the ambient tunnel pressure measured on the body above.

5. Tunnel Nonuniformities

Nonuniformities in the tunnel flow field, though small, introduce some errors in the pressure readings. This is in contrast to the case which will usually be encountered in free flight where the free-stream flow can be treated as uniform. The presence of these tunnel nonuniformities means that when the body alone is introduced into the flow the pressures recorded on the body will not in general be correct. Actually the pressure as measured on the body alone at any one orifice will be composed of several parts and may be written as

$$p_{measured} = p_{body\ alone} + \Delta p_{induced}\ , \qquad (1)$$

where $p_{body\ alone}$ is the pressure on the body alone in a uniform stream and is a function only of the geometry of the particular body under consideration, and $\Delta p_{induced}$ is the incremental pressure induced on the body alone due to the tunnel nonuniformities and is a function of both the body geometry and the tunnel nonuniformities.

For the particular body used in these tests considerable care was taken to keep the value of $p_{body\ alone}$ as constant as possible; i.e., the pressure variation in x has been minimized. The use of a long hollow body insures that for all practical purposes there will be no axial pressure gradients on the body at zero angle of attack due to the body shape. Since the body field moves with the body, and hence with the orifice pattern, the effect of a nonconstant $p_{body\ alone}$ is to cause a consistent difference between the pressures read at different orifices for the same axial position.

Over most of the orifice region $\Delta p_{induced}$ is small, since the tunnel nonuniformities are small. For small disturbances the tunnel field is fixed with respect to the tunnel, which causes differences between the pressures read by any one orifice for successive axial positions.

If the wing is introduced into the flow the measured pressure becomes

$$p_{measured} = p_{body\ alone} + \Delta p'_{induced} + \Delta p_{interference}\ , \qquad (2)$$

where $p_{body\ alone}$ is defined as above, $\Delta p'_{induced}$ is the pressure induced on the body in the presence of the wing by the nonuniform flow, and $\Delta p_{interference}$ is the pressure induced on the body due to the presence of the wing in a uniform flow. If $\Delta p_{interference}$, $\Delta p_{induced}$, and $\Delta p'_{induced}$ are small quantities, then the linear theory applies and $\Delta p_{induced} = \Delta p'_{induced}$, so that a simple subtraction of the pressures on the body alone from those on the body in the presence of the wing gives the desired result, namely $\Delta p_{interference}$. If, however, $\Delta p_{induced}$, $\Delta p'_{induced}$, and $\Delta p_{interference}$ are not sufficiently small, there will be some interaction between them and a simple subtraction will not give $\Delta p_{interference}$.

Figure 2 shows the raw experimental data obtained from the row of orifices in the meridional plane $\theta = +10°$, on both the body alone and the body in the presence of the wing at -8° angle of attack. The sharp bump in the body-alone pressure curve indicates that a weak shock wave which deflects the flow 3° strikes the body 1/2 inch aft of the tunnel centerline. A similar bump in the pressure curve on the body in the presence of the wing occurs, but its position is shifted 1/4 inch forward. This axial shift is due to the fact that the tunnel shock bends forward after intersecting the shock wave from the wing leading edge; i.e., there is some interaction between $\Delta p_{induced}$ and $\Delta p_{interference}$.

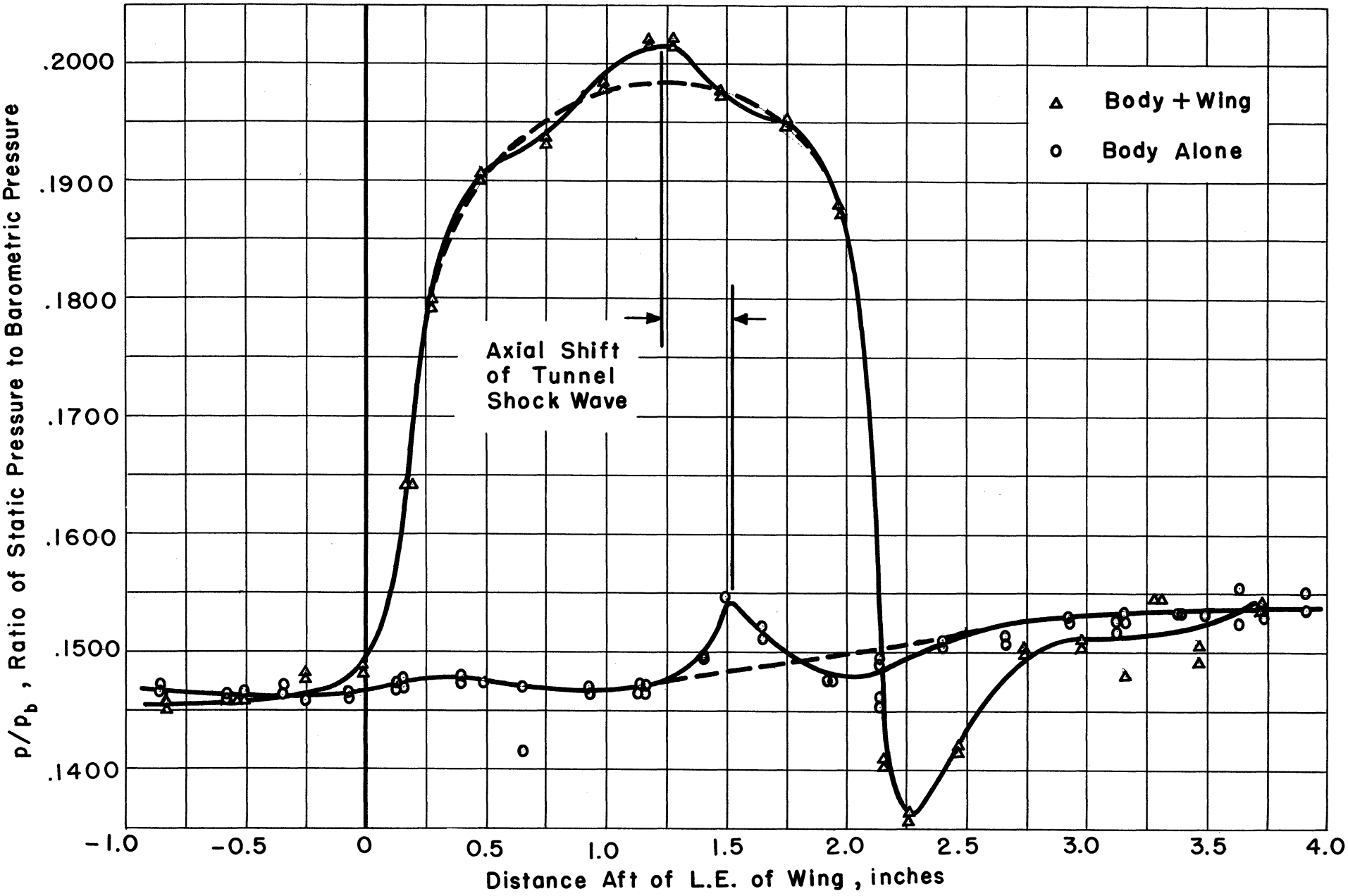

Fig.2. Sample of Raw Experimental Data

If the tunnel shock were not present, the body-alone curve would follow the dotted line which is tangent to the actual body-alone pressure curve. Furthermore, in the absence of the tunnel shock, the pressure curve on the body in the presence of the wing would be given by the dotted line faired between the experimental points. The difference between the faired pressure curves for the body and the body plus the wing then represents the interference effect of the wing on the body.

All the experimental pressure profiles presented in this report have been treated in the above manner in order to eliminate as far as possible the effect of flow-nonuniformities.

D. EXPERIMENTAL RESULTS

1. Body Alone at Zero Angle of Attack

If the effect of the wing on the body is desired, it is necessary first to obtain the pressure distribution and flow characteristics for the body alone. As was mentioned in section C,2 the body was designed to obtain a pressure field as nearly constant as possible. The very weak shock waves from the nose and the turbulence wire reflect from the ceiling and the floor, and strike the body aft of the orifice pattern as indicated by schlieren photographs of the body alone. Furthermore, the reflections of these weak shock waves from the tunnel sidewalls strike the body forward of the orifice region, as indicated by the china-clay pattern for the body alone. Hence, the pressure field for the body alone appears to be quite constant in the orifice region when the long nosepiece and the spacer are used.

As is evident from both the china-film pattern and the static-pressure distributions (Fig. 2) on the body alone, the weak shock wave mentioned in section C,5, which probably originates at the juncture between the access window and the main window (Fig. 1), strikes the body 1/2 inch aft of the tunnel centerline in the meridional plane $\theta = 10°$. As higher or lower values of θ are considered this effect moves aft along the body approximately along the elliptical path formed by the intersection of the Mach plane from the juncture and the cylindrical body.

With the long nose and the spacer in position, the orifice region lies approximately 12 inches aft of the nose. At this point the calculated boundary-layer thickness, assuming turbulent boundary-layer flow from the nose, should be 0.22 inch using the formula $\delta = 0.37x/[Re]^{\cdot 2}$ and a Reynolds number of 3.6×10^6. This formula for δ is based on experimental results[15] and assumes incompressible

flow. Actual measurements of the boundary-layer thickness from schlieren photographs show that the boundary-layer thickness is between 0.18 inch and 0.24 inch. This apparent variation of the boundary-layer thickness does not occur from one run to another, but rather is indicative of the difficulty encountered in measuring the boundary-layer thickness from schlieren photographs.

2. Body at Zero Angle of Attack and Flat Surface of the Wing at Angle of Attack

The pressure distributions for the body at zero angle of attack in combination with the wing at angles of attack of $\pm 4°$ and $\pm 8°$ are plotted in Fig. 3 for various values of θ. Figure 4 is a composite plot of the experimental pressure profiles for various values of θ when the wing is at -8 and +8° angle of attack. All these experimental curves were obtained by taking the difference between the pressure profiles of the body alone and the body in combination with the wing as illustrated in section C,5. The results have been nondimensionalized and made independent of both the angle of attack and the Mach number by plotting $\beta C_p/\alpha_w$ vs. x/β. In the meridional planes $\theta = 0°$ and $\theta = 5°$, the pressure data available were insufficient to permit the presentation of pressure profiles because some of the orifices in these planes were covered by the wing for some axial body positions.

Since in the linearized theory the wing boundary conditions are not applied in the wing plane, but rather in the plane $\theta = 0°$, no account is taken of the foreshortening effect due to angle of attack. Figure 5 shows that for a negative angle of attack of 8° the area on the body between the Mach helix from the leading-edge juncture and the Mach helix from the trailing-edge juncture is shortened by an amount $x/\beta = 0.17$. On the other hand, for an angle of attack of +8° this area is lengthened by the same amount. For an angle of attack of $\pm 4°$ the shortening or lengthening will be $x/\beta = 0.085$.

a. Wing at Negative Angles of Attack. For negative angles of attack there will be a compression over the flat surface of the wing. The effect of the presence of a turbulent boundary layer on the body is to permit the upstream propagation of the pressure rise due to this wing leading-edge shock. If the boundary-layer thickness is taken to be 0.2 inch, and if the corrections indicated in the preceding section are made, it is found that the upstream propagation varies from about 3 boundary-layer thicknesses in the plane $\theta = 10°$ to about 9 boundary-layer thicknesses in the plane $\theta = 90°$ for the wing at -8° angle of attack. At -4° angle of attack this upstream propagation is approximately the same as for the -8° angle of attack. This variation in the distance of upstream propagation with θ is due to the boundary-layer crossflow, which causes a thicker boundary layer for larger values of θ. Thus, the overall viscous effect at the leading edge is to smooth out the steep pressure rise associated with the shock wave; the amount of smoothing out increases for larger values of θ.

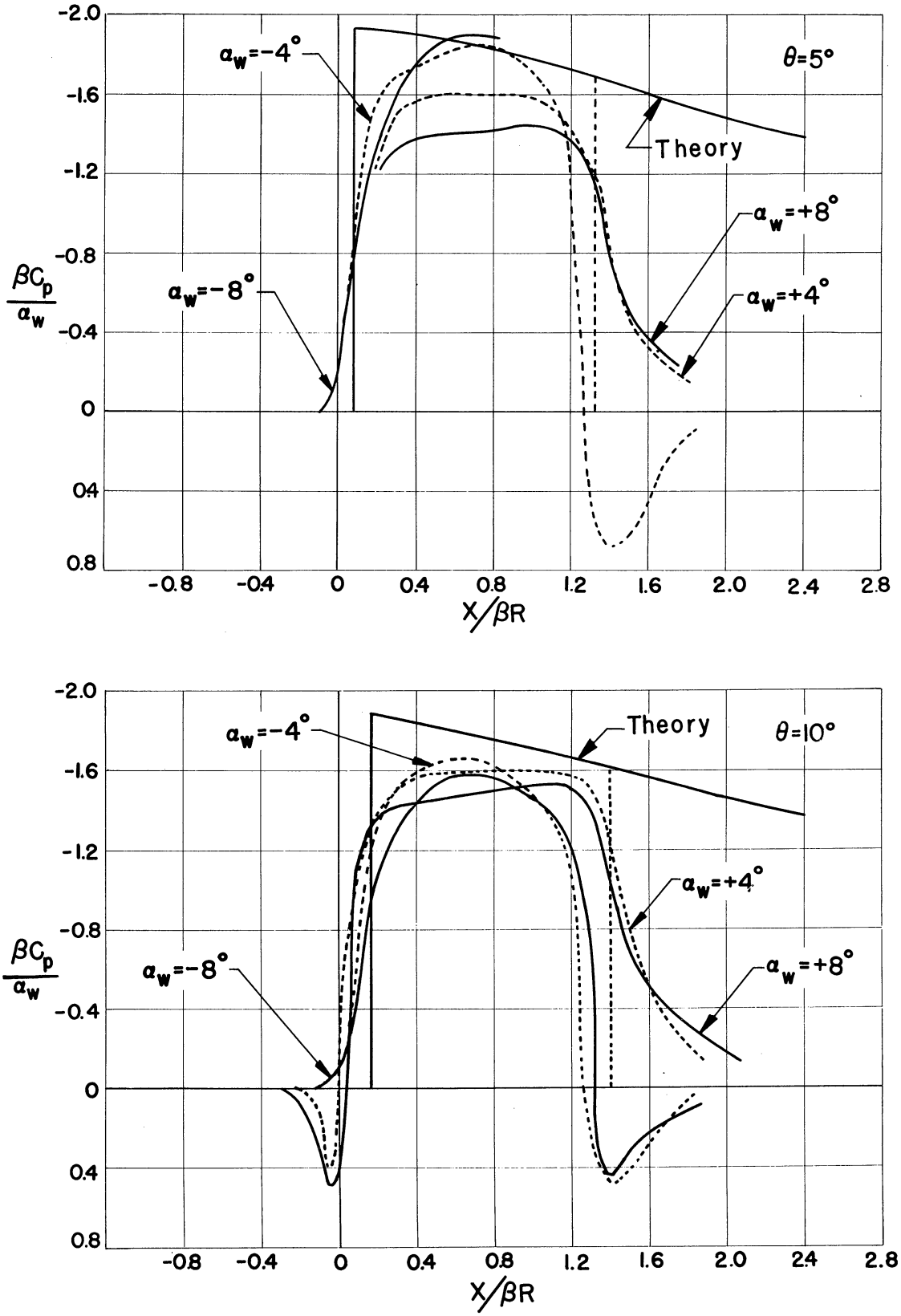

Fig. 3—Pressure profiles: $\alpha_B = 0$, $\alpha_w = \pm 4°, \pm 8$, flat surface of the wing.

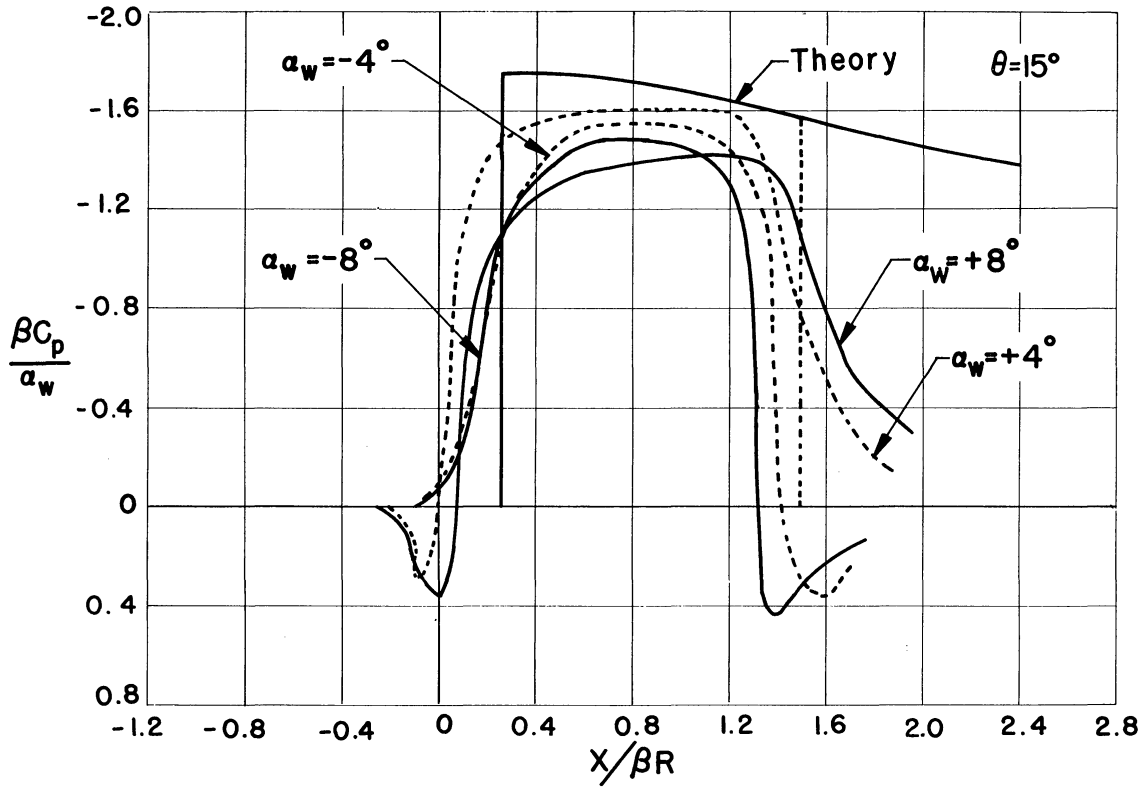

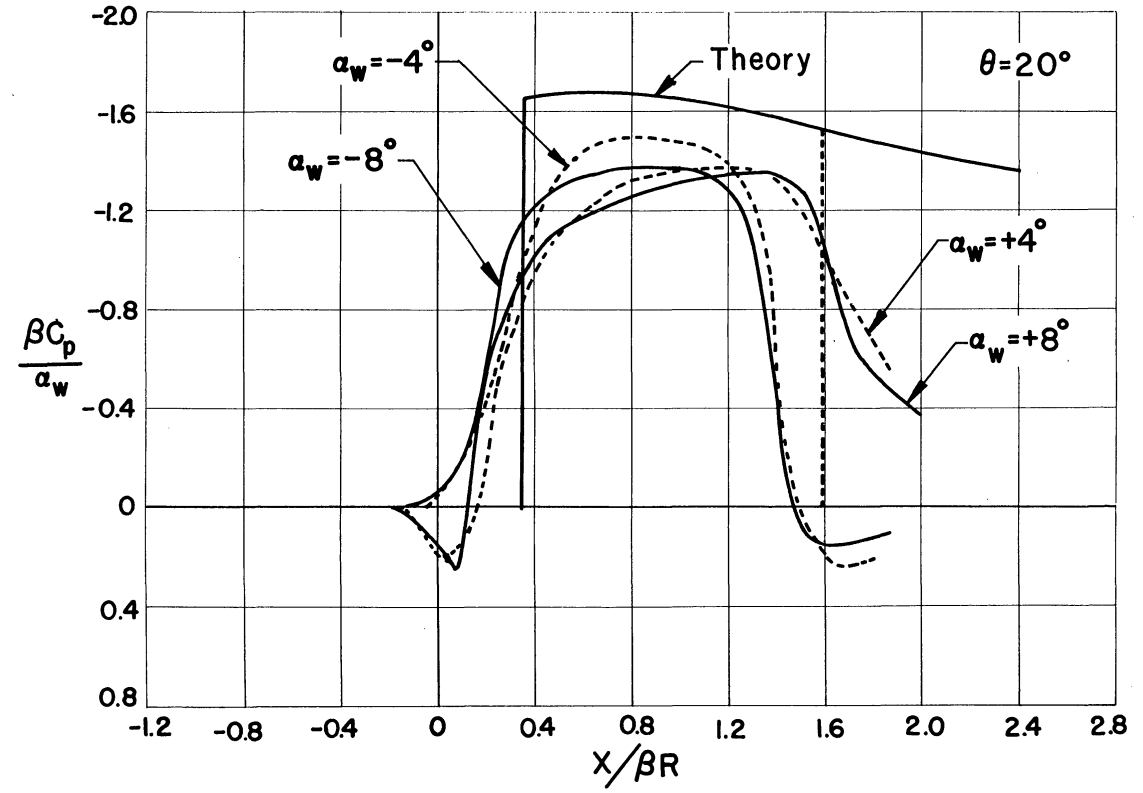

Fig. 3 (Continued)

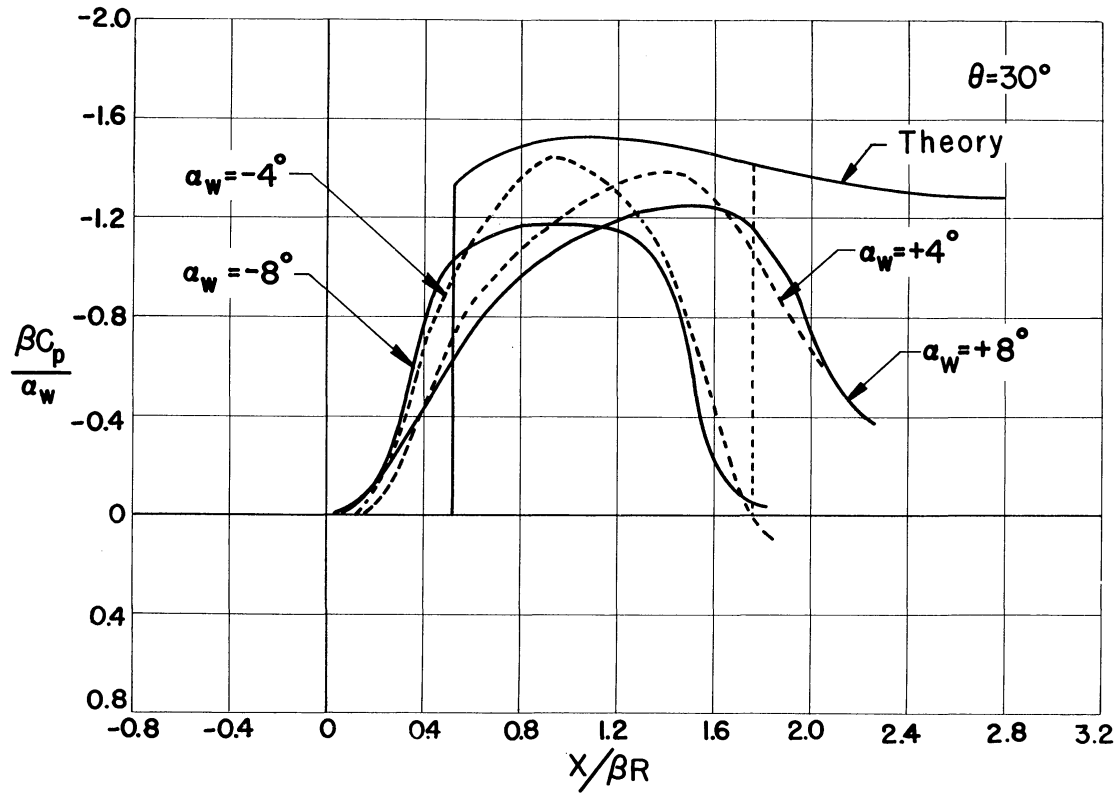

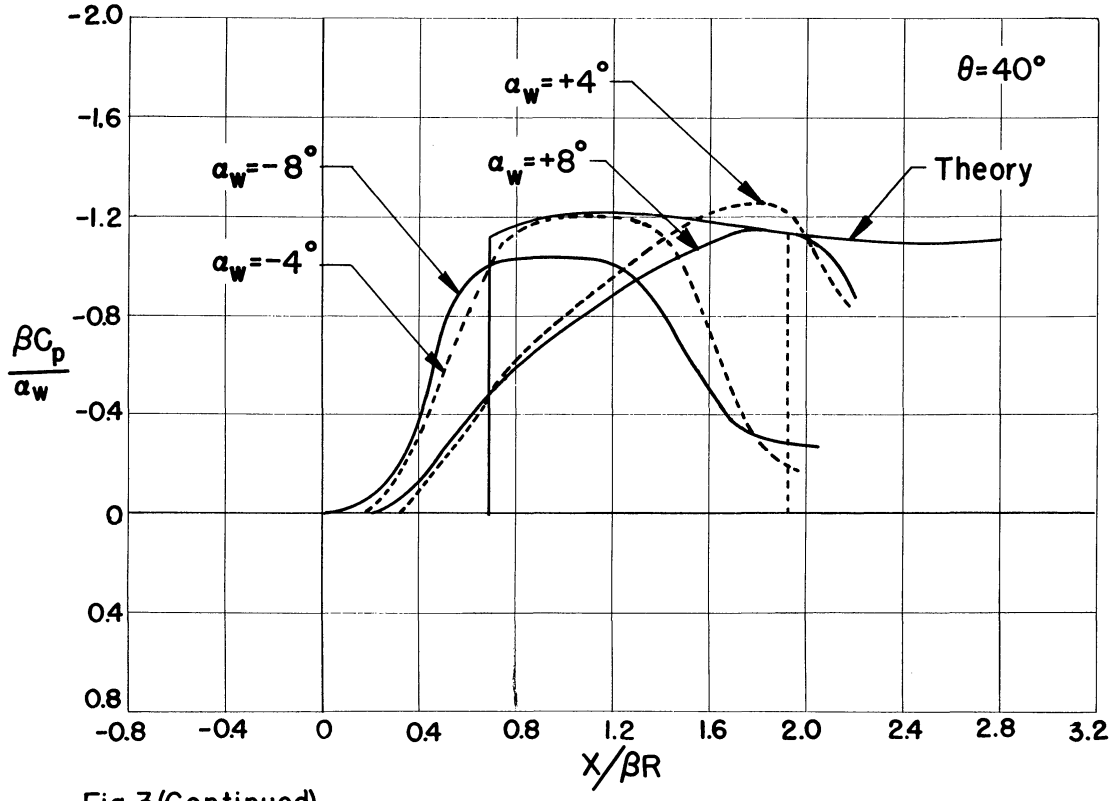

Fig. 3(Continued)

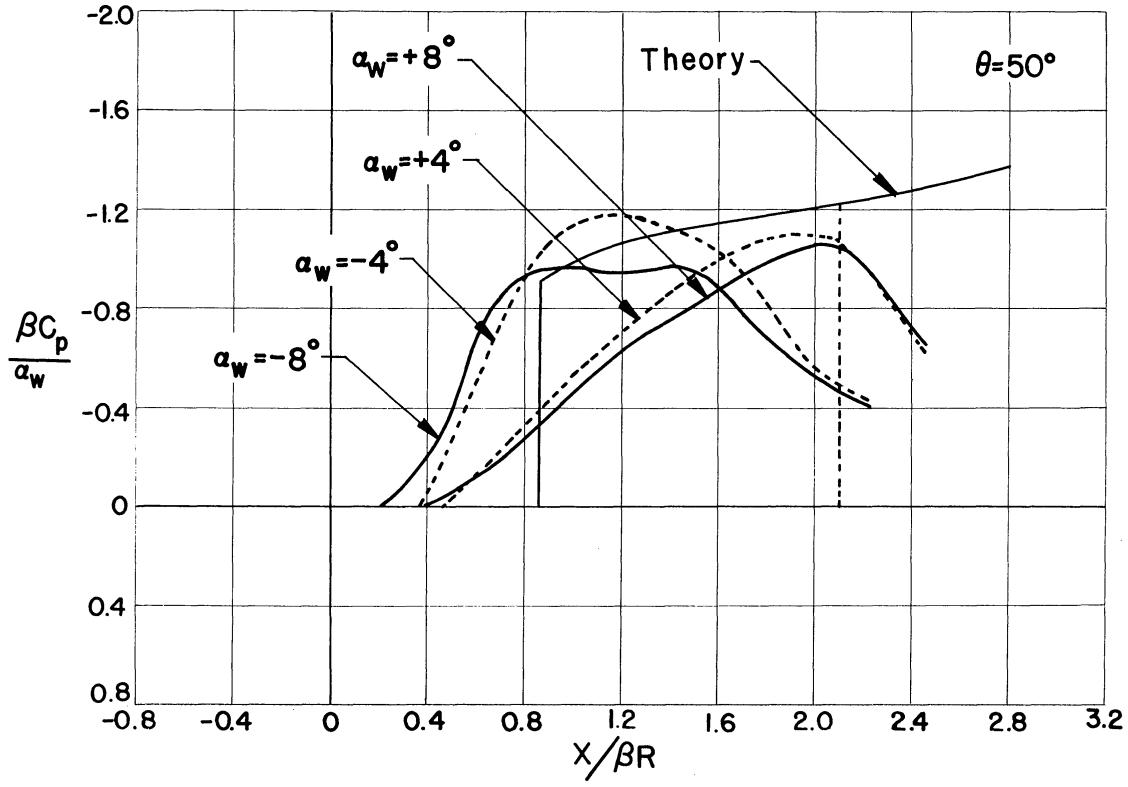

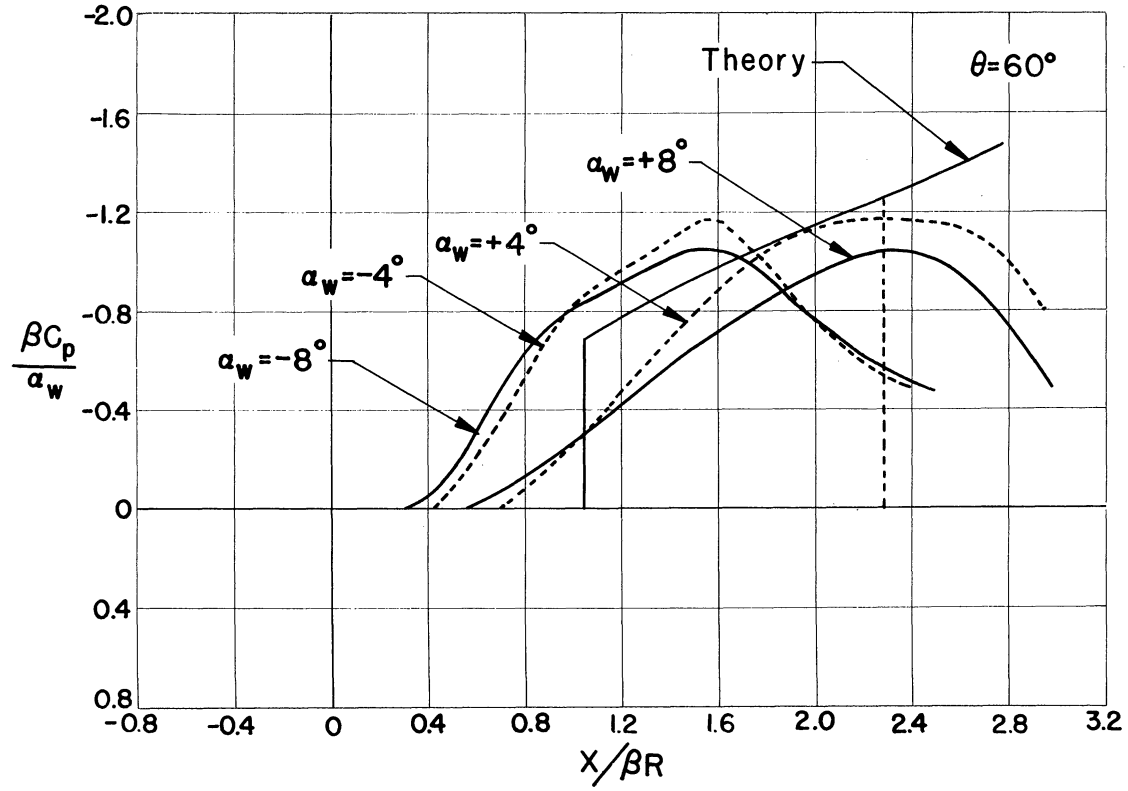

Fig. 3 (Continued)

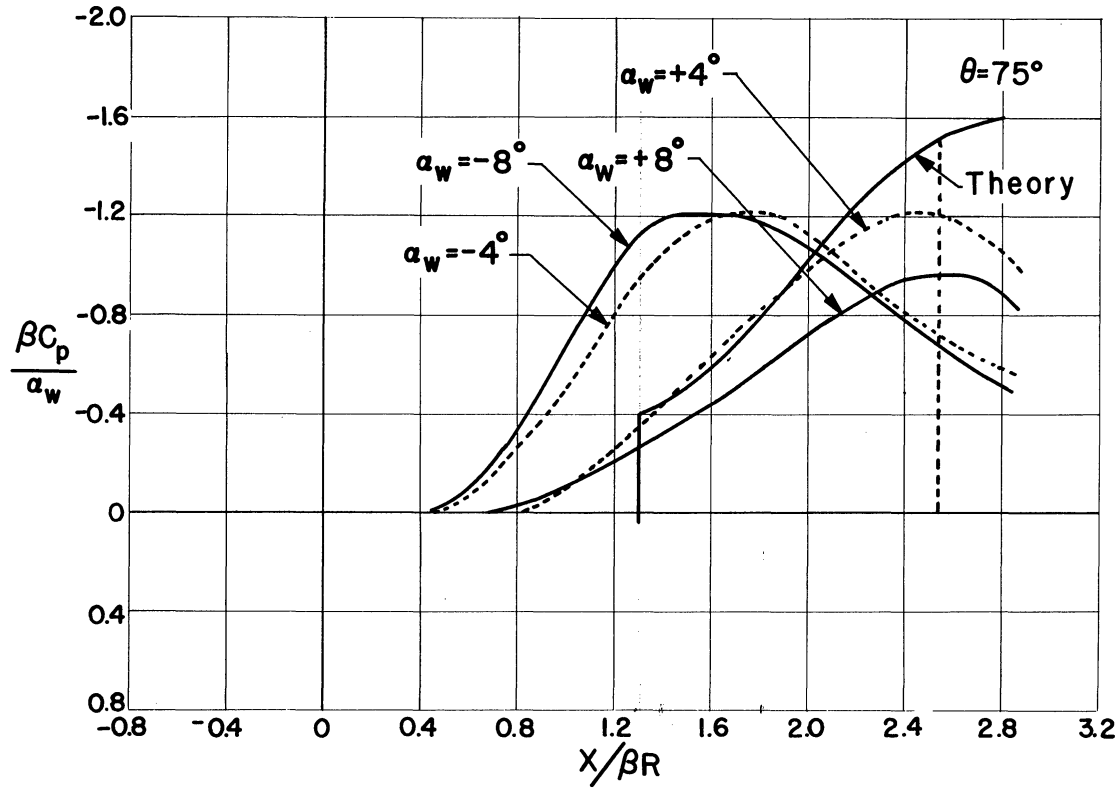

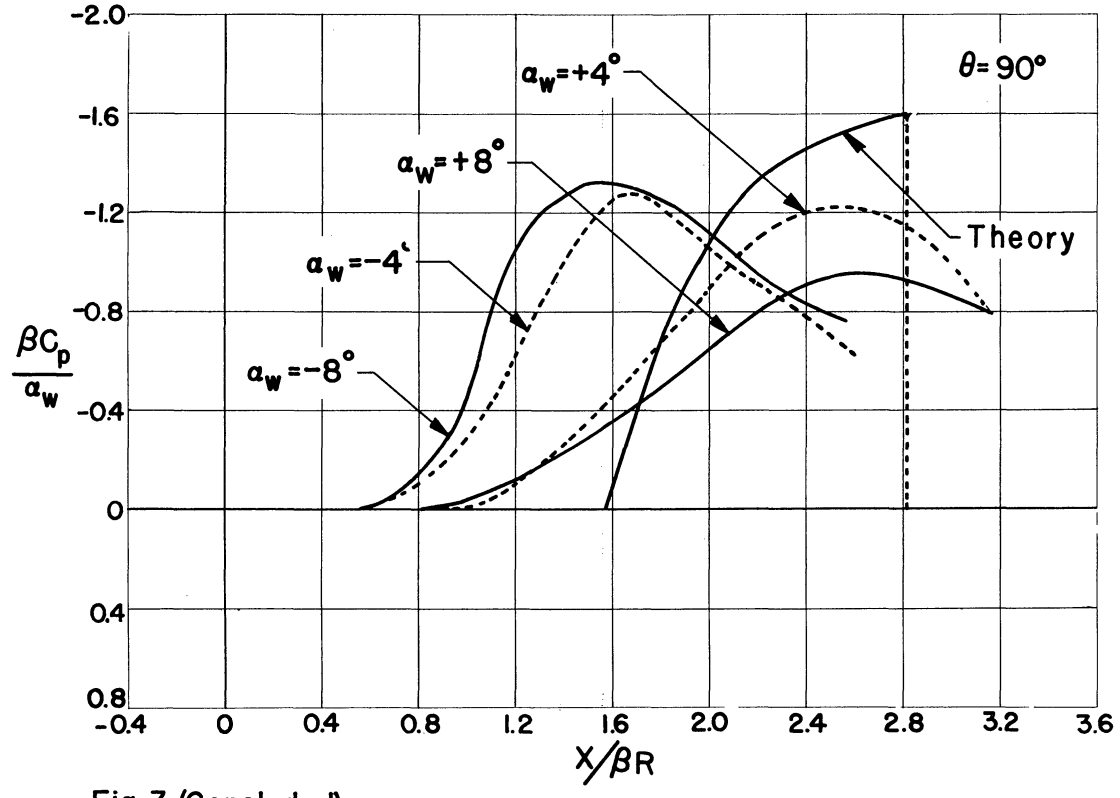

Fig. 3 (Concluded)

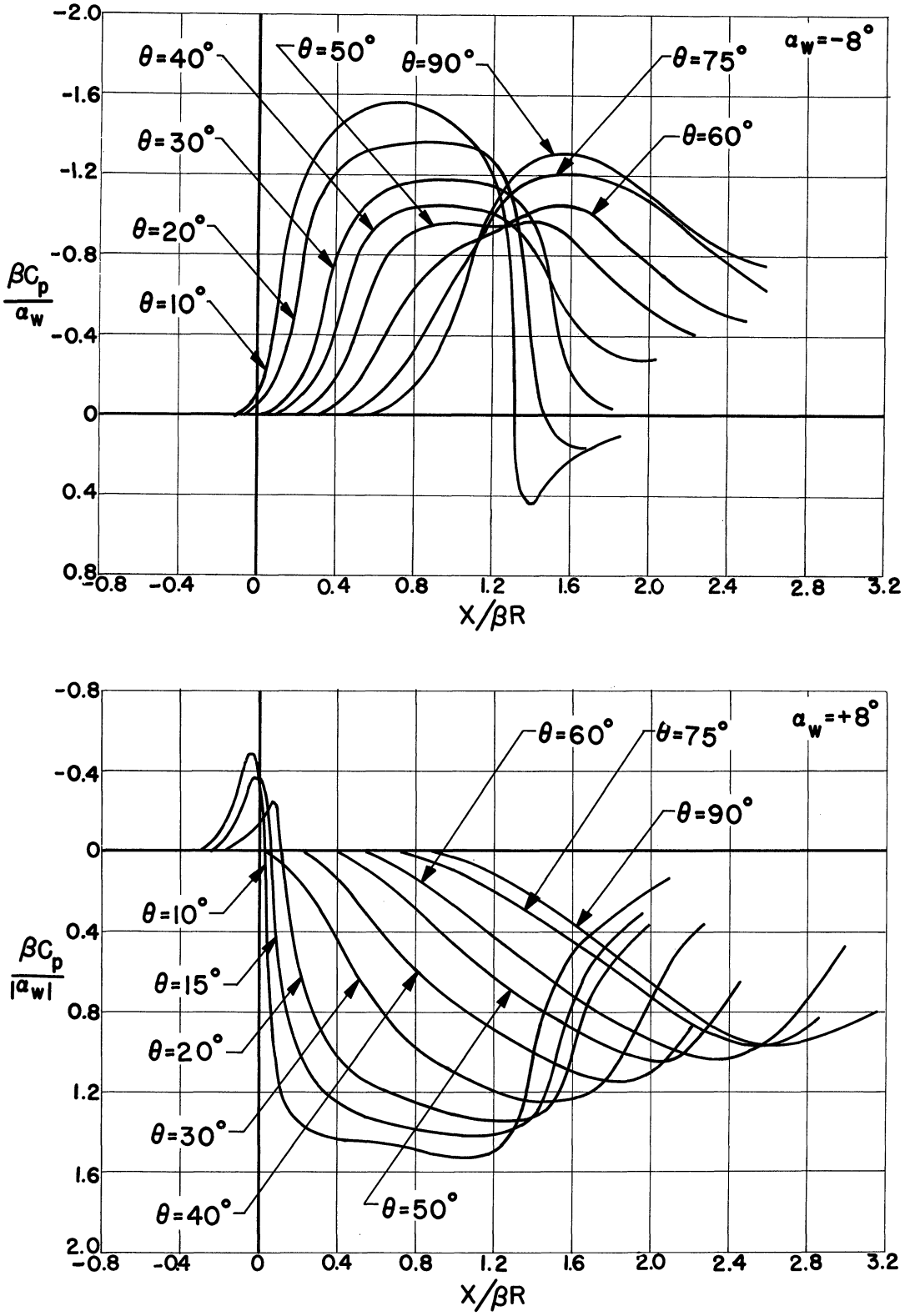

Fig. 4 — Composite pressure profiles: $\alpha_B = 0, \alpha_W = \pm 8°$, flat surface of the wing.

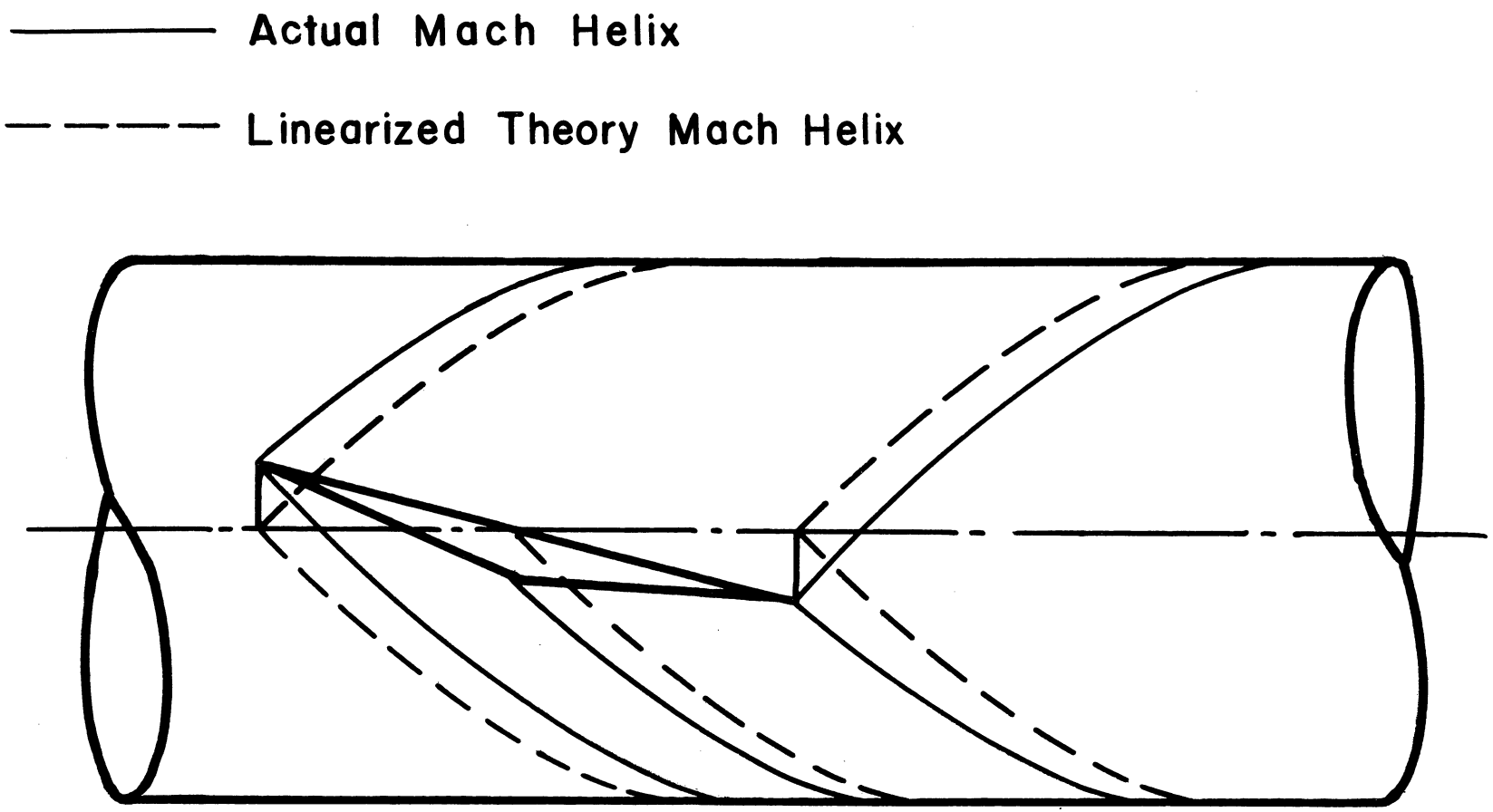

Fig. 5. Effect of Wing Incidence on the Region of the Body Influenced by the Wing.

Aft of the leading-edge shock wave the pressure curves agree fairly well with the linearized theory, until slightly ahead of the point at which the trailing-edge effect appears according to linearized theory. This point is indicated by the vertical dotted lines in Fig. 3. The experimental curves indicate that at this point there is a sharp decrease in pressure due to the expansion wave at the wing trailing edge. For the smaller values of θ (i.e., $\theta < 30°$) this expansion is actually larger than the compression which occurs at the leading edge, so that the pressure curves overshoot the ambient pressure and then begin to approach it assymptotically from below. A strong shock wave, which originates at the outboard wing support, begins to influence the body pressures 1 inch downstream of the wing trailing edge; the exact assymptotic behavior of the pressure curves is therefore uncertain.

Theoretically, as the shock wave moves around the cylinder its strength is continuously attenuated, until at the top meridian the shock jump is zero. However, this shock jump represents only a part of the theoretical pressure rise, since the total pressure rise is made up of the shock jump plus a continuous axial pressure gradient due to the interference potential field.

If planes x/β = constant (Fig. 4) are considered, a rather strong lateral pressure gradient will be noticed for increasing values of θ. This gradient causes a strong boundary-layer crossflow toward the top meridian. As a matter of fact china-clay patterns observed on the flat compression surface of the wing (Fig. 7) indicate that some of the wing boundary-layer air will be swept from the wing onto the body and then toward the top meridian.

Since the entire flow picture is symmetrical with respect to the plane $\theta = 90°$, it is apparent that there will be an accumulation of the slow-moving boundary-layer air at the top of the body. This accumulation is clearly visible in the schlieren picture, Fig. 6. Other evidence of this boundary-layer crossflow may be found in the china-clay pattern of Fig. 7. The effect of this accumulated boundary layer will be to form a wedge-shaped obstacle of slow-moving air which will result in a relatively slow increase in pressure at the high meridional angles. As the compressive waves proceed downstream and outward, they will coalesce into a compression shock as indicated in the schlieren photograph, Fig. 6.

b. Wing at Positive Angles of Attack. For positive angles of attack there will be an expansion wave originating at the wing leading edge. This expansion wave is preceded for small values of θ (i.e., $\theta < 30°$) by a very slight compression, as mentioned in section B,2. The presence of this small compression is evident both on the pressure profiles of Figs. 3 and 4 and on the china-clay pattern of Fig. 8.

The upstream propagation of the expansion-wave disturbance through the turbulent boundary layer is about three boundary-layer thicknesses in the

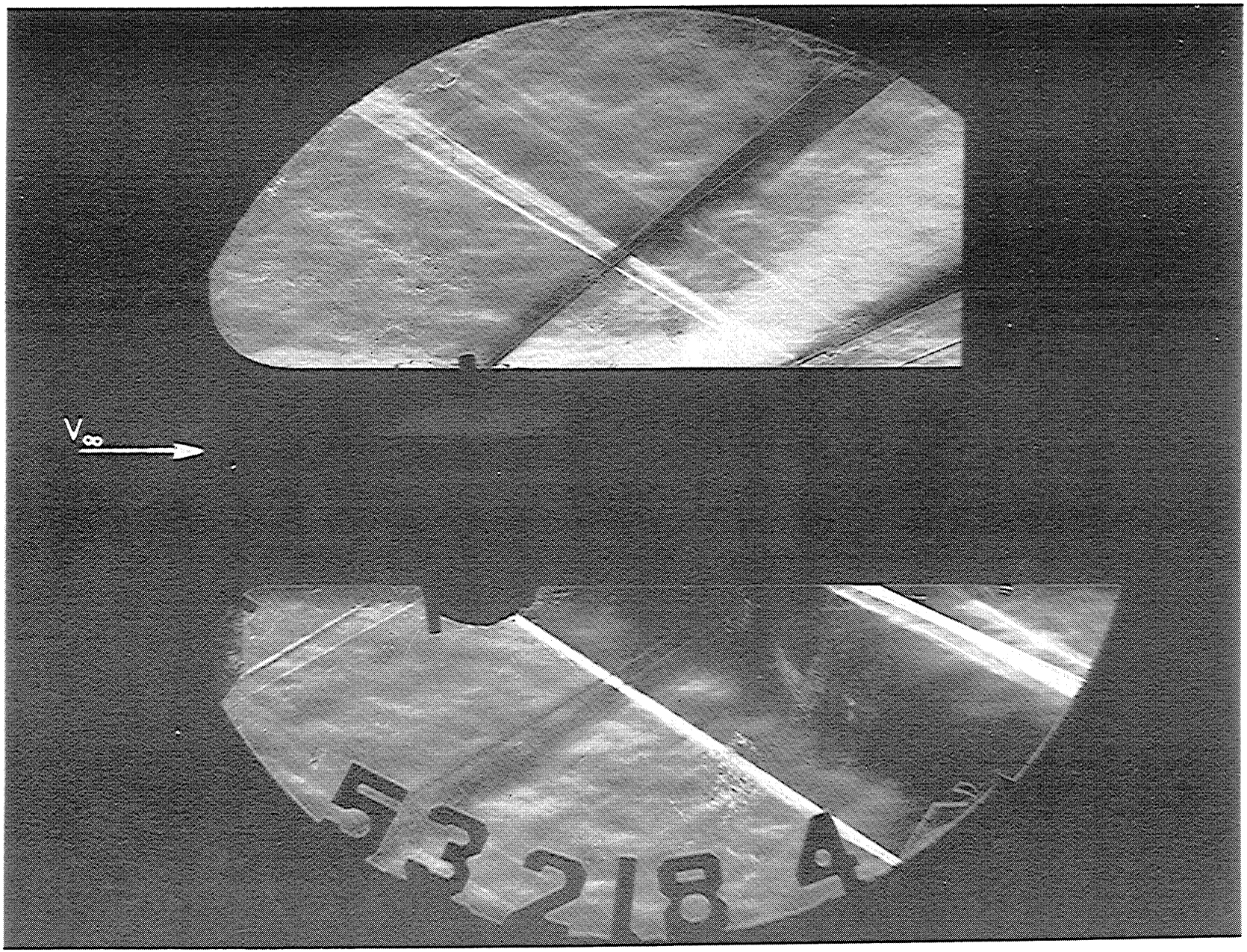

Fig. 6. Schlieren photograph: $\alpha_B = 0°, \alpha_W = -8°$.

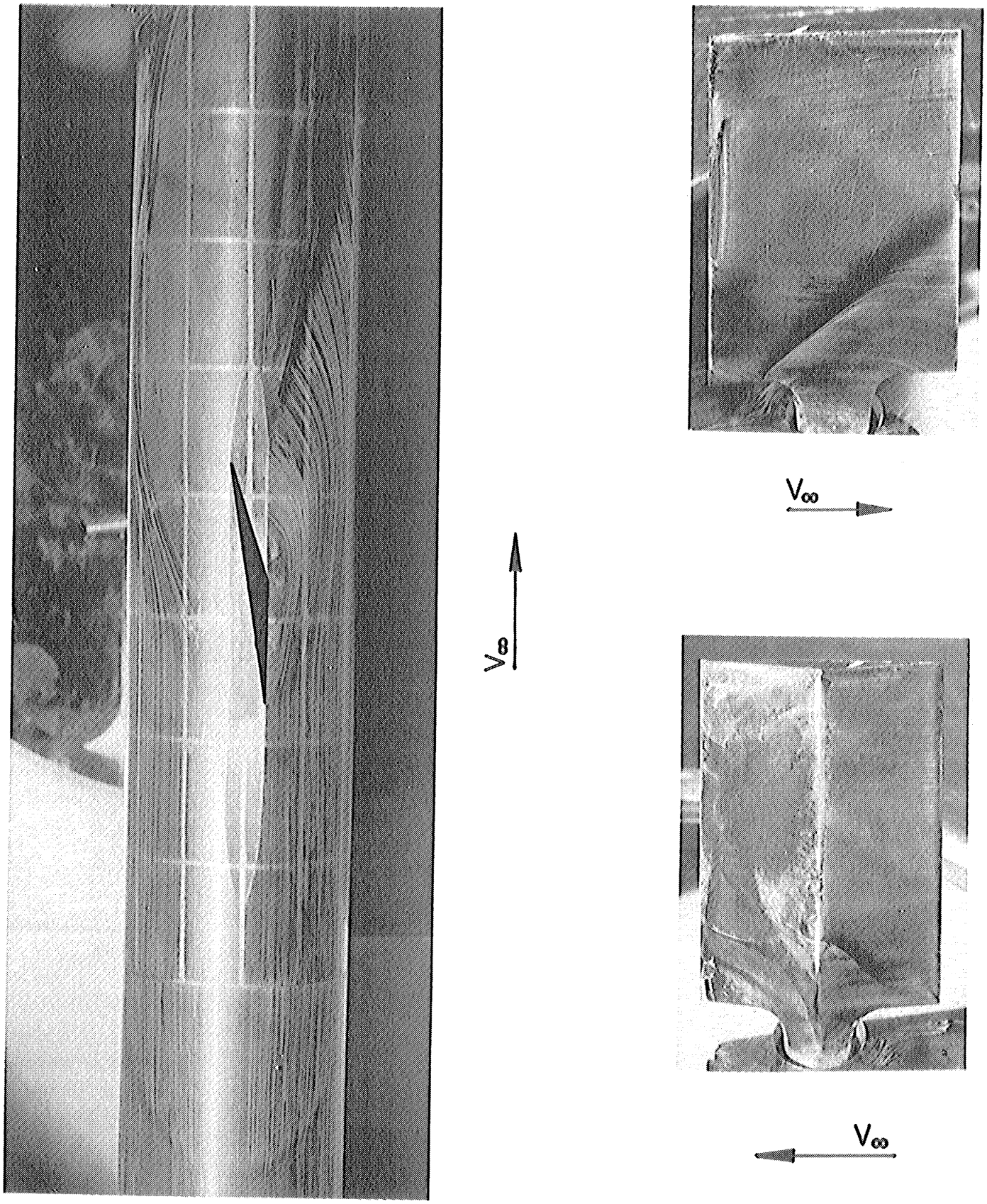

Fig. 7. China clay photograph: $\alpha_B = 0°, \alpha_W = -8°$.

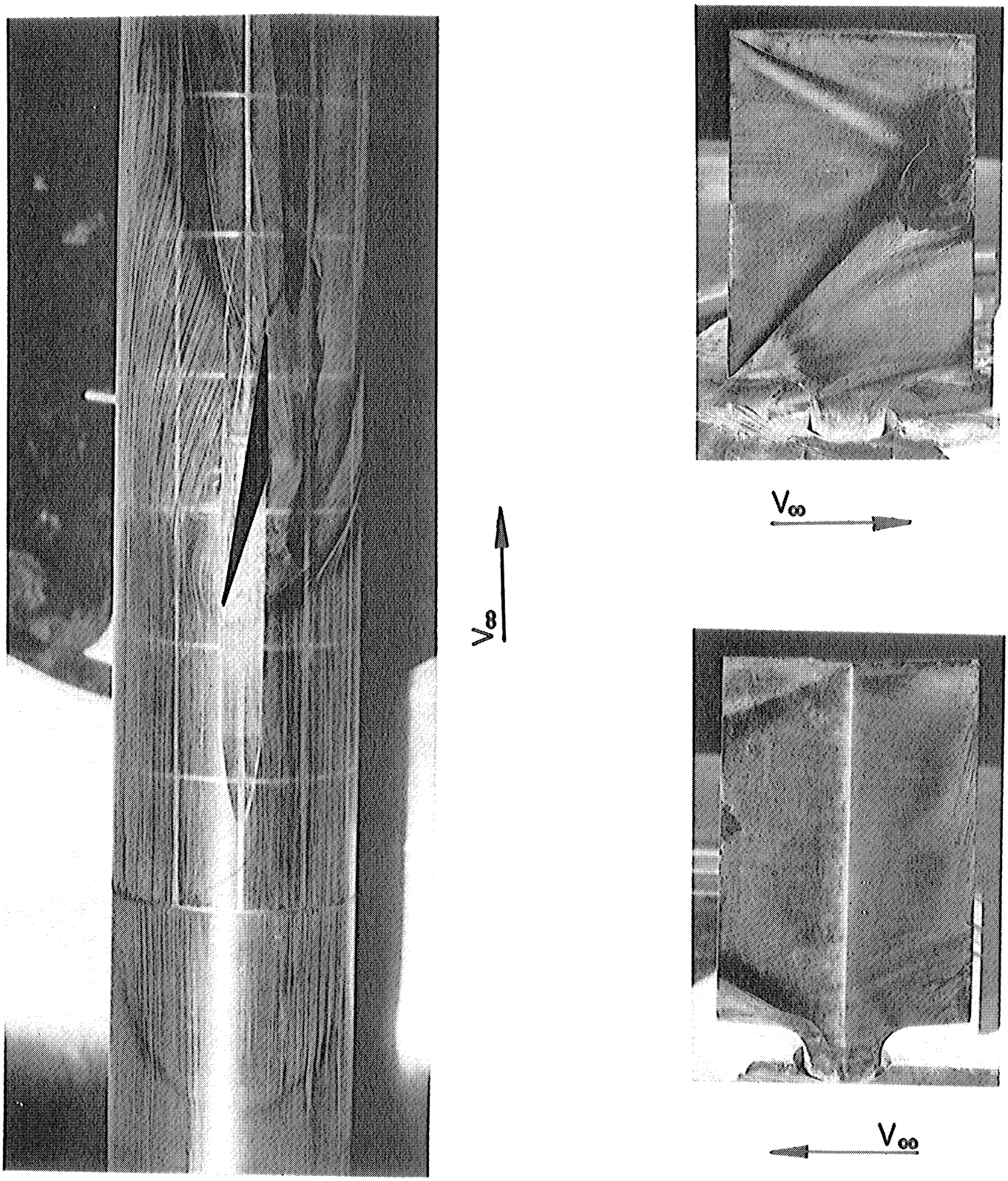

Fig.8. China clay photograph: $\alpha_B = 0°, \alpha_W = +8°$

meridional plane $\theta = +10°$, and about six boundary-layer thicknesses at the top meridional plane, $\theta = 90°$. For the smaller values of θ (i.e., $\theta \leq 20°$) the pressure drop on the body due to the expansion wave is as steep as the pressure rise due to the compression shock which occurs for negative angles of attack. However, for values of $\theta > 20°$ the pressure drop becomes less steep, since the expansion wave, unlike the compression shock, takes place over an increasing axial distance for the higher values of θ. In the plane $\theta = 90°$ the pressure drop is quite gentle and is spread out over a distance $x/\beta = 1.6$, as compared to the pressure rise in the compression case, which takes place in a distance $x/\beta = 1.0$.

The pressure gradients on the body, as shown for constant values of x/β in Fig. 4, tend to force the boundary layer away from the top meridian $\theta = 90°$ and toward the wing plane, producing a flow of air onto the wing from the body. The schlieren photograph (Fig. 13) for this configuration indicates that the boundary layer does become somewhat thinner at the top meridian.

Figure 8, which is the china-clay pattern of the flat expansion side of the wing, clearly shows a separated region at the wing trailing edge. This separation is probably triggered by the confluence of the strong distrubances originating at the juncture of the body and wing leading edge and at the outboard wing tip. The disturbance which comes from the juncture of the body and wing leading edge is of the shock-expansion-shock type and is probably caused by a bump or local thickening in the body boundary layer just ahead of the wing leading edge. This bump in the body boundary layer is in turn caused by the strong shock from the wedge-surface (compression) side of the wing. The disturbance, which originates at the outboard wing tip appears to separate the flow, at least locally, so that the high-pressure air from the bottom (compression) side of the wing flows around the wing's outboard edge and onto the top (expansion) side of the wing.

Close to the body and for a distance of about 1/2 inch outboard, Fig. 8 indicates that the flow definitely follows the wing to the trailing edge in spite of the trailing-edge shock.

The trailing-edge shock, the trace of which is clearly visible on the body china-clay patterns, appears to deflect the boundary layer back to approximately the free-stream direction. The pressure distributions aft of the wing trailing edge are affected by the strong disturbance which originates at the outboard wing tip and strikes the body at a point about 1 inch aft of the trailing edge.

3. Wedge Surface of the Wing

With the wing section used in these tests, it is possible to obtain the effect of the simplest type of cambered wing on wing-body interference

simultaneously with the effects just described for a flat surface wing. Actually, it is impossible to isolate completely the effects of the two sides of the wing experimentally at the leading edge; e.g., the remarks in the previous section concerning the disturbance on the flat-surface side of the wing at +8° angle of attack, which originates at the juncture of wing leading edge and the body, indicated that this disturbance was a result of the high pressures on the wedge surface of the wing. Furthermore, both the inviscid linearized flow and the experimentally observed flow aft of the wing trailing edge are obviously related to the wing cross section used.

Composite pressure distributions in the form of $\beta\, C_p/8°$ plotted versus x/β for wing angles of attack of +8, 0, and -8° are shown in Figs. 9 and 10. Figure 11 shows a comparison between the experimental pressure profiles obtained with the wing at zero angle of attack and the theoretical linearized solution. The theoretical curves are easily obtainable from the results of reference 1 by superimposing the theoretical curves for a wing at -10° angle of attack on similar theoretical curves displaced 1/2 chord length for a wing at +20° angle of attack.

With the wing at -8° angle of attack, the flow is deflected 2° by a weak compression shock at the leading edge. The disturbance is small but the resulting upstream propagation is still about 6 boundary-layer thicknesses in the 90° meridionial plane. The china-clay pattern shows that there is little boundary-layer crossflow resulting from this leading-edge shock wave. At the midchord point, which is also the point of maximum camber, the flow over the wing should be deflected 20° by an expansion wave. Actually, china-clay patterns on the wing indicate that the flow separates from the wing at the midchord point over the entire wing span, except for the most inboard wing stations. The fact that the flow near the surface of the body does appear to be deflected through the full 20° is borne out by the china-clay pattern of Fig. 8. Therefore it appears that at the most inboard sections of the wing, which lie in the body boundary layer, the flow follows the wing contour, whereas over the entire outboard portion of the wing the flow fails to turn through the full 20° and separates from the wing at the midchord point. Regardless of the exact lateral extent of the separation, it is apparent from the pressure profiles that the actual expansion over the aft half of the wedge surface of the wing does not reach the theoretical value. It is possible that if the flow in the wing boundary layer were turbulent over the outboard sections of the wing, then the flow would be turned through the full 20° of expansion and follow the wing surface up to the trailing edge.

The results obtained for a wing with camber only are shown in Figs. 9 and 11. The upstream propagation of the compressive disturbance generated by the compression shock at the wing leading edge is about 9 boundary-layer thicknesses in the 90° meridian plane, which is the same as that observed for the flat

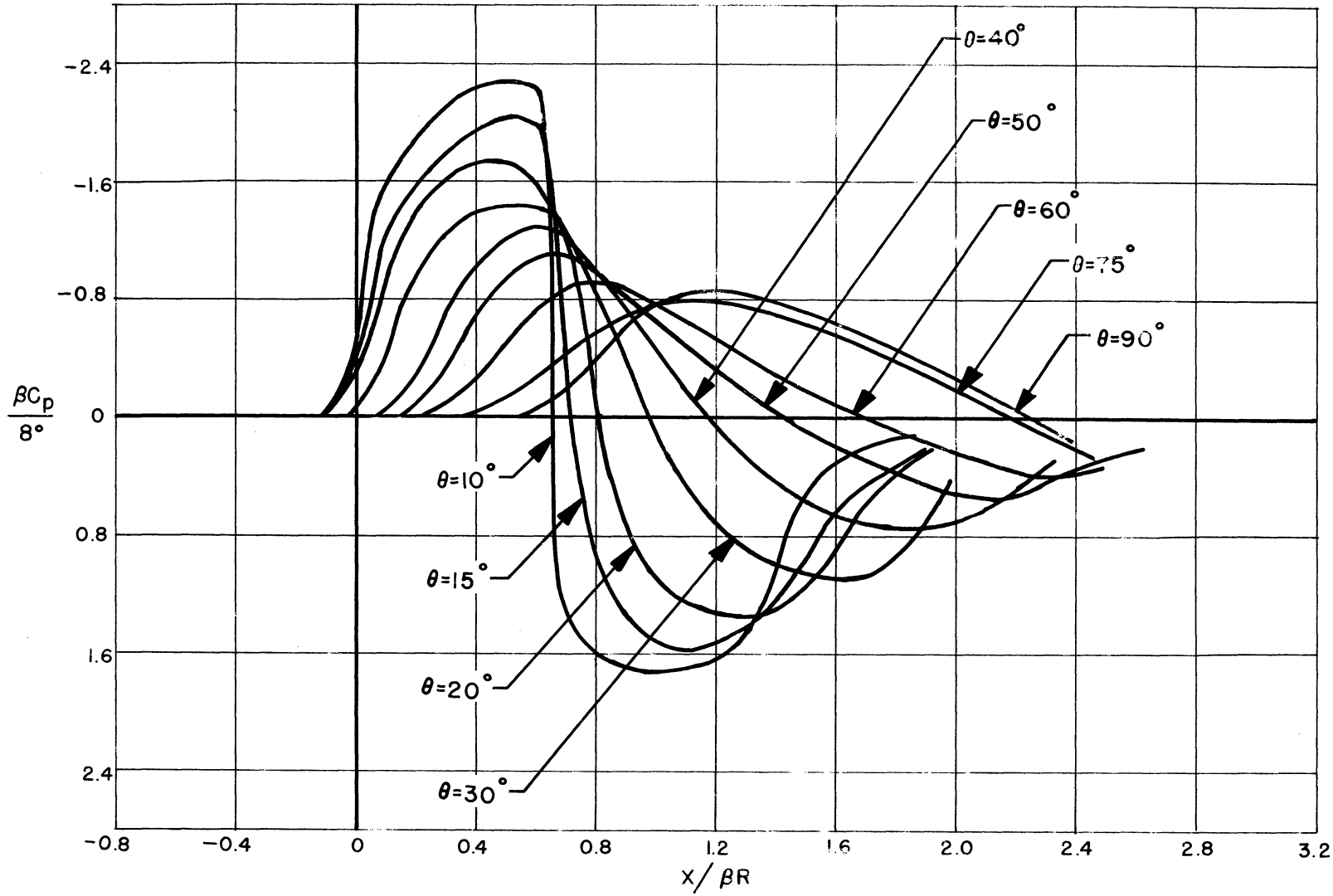

Fig.9—Composite pressure profiles: $\alpha_B=0$, $\alpha_W=0$, wedge surface of the wing.

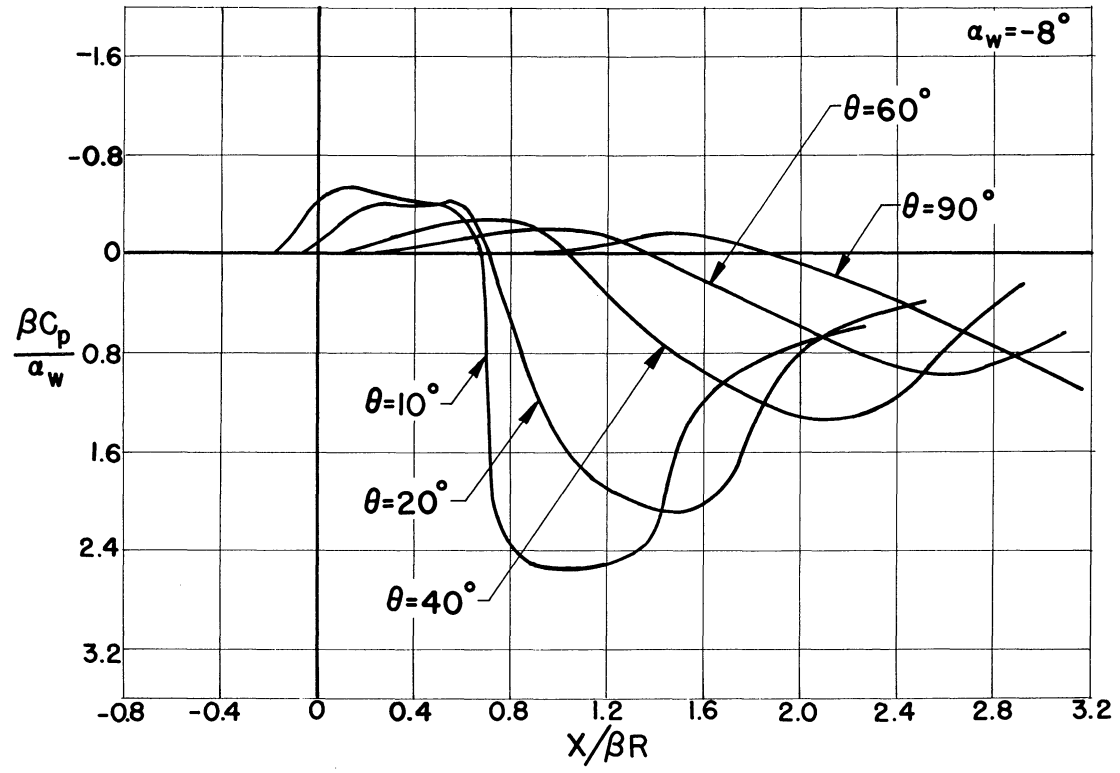

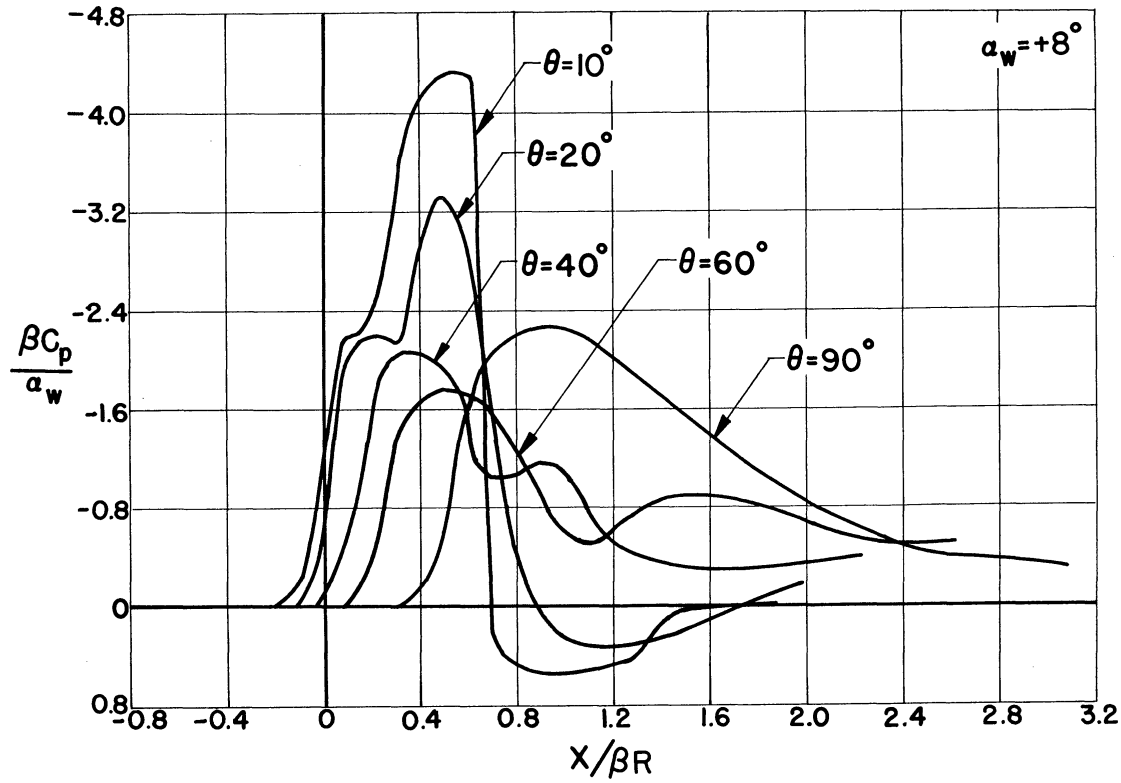

Fig. 10—Composite pressure profiles: $\alpha_B = 0$, $\alpha_w = \pm 8$, wedge surface of the wing

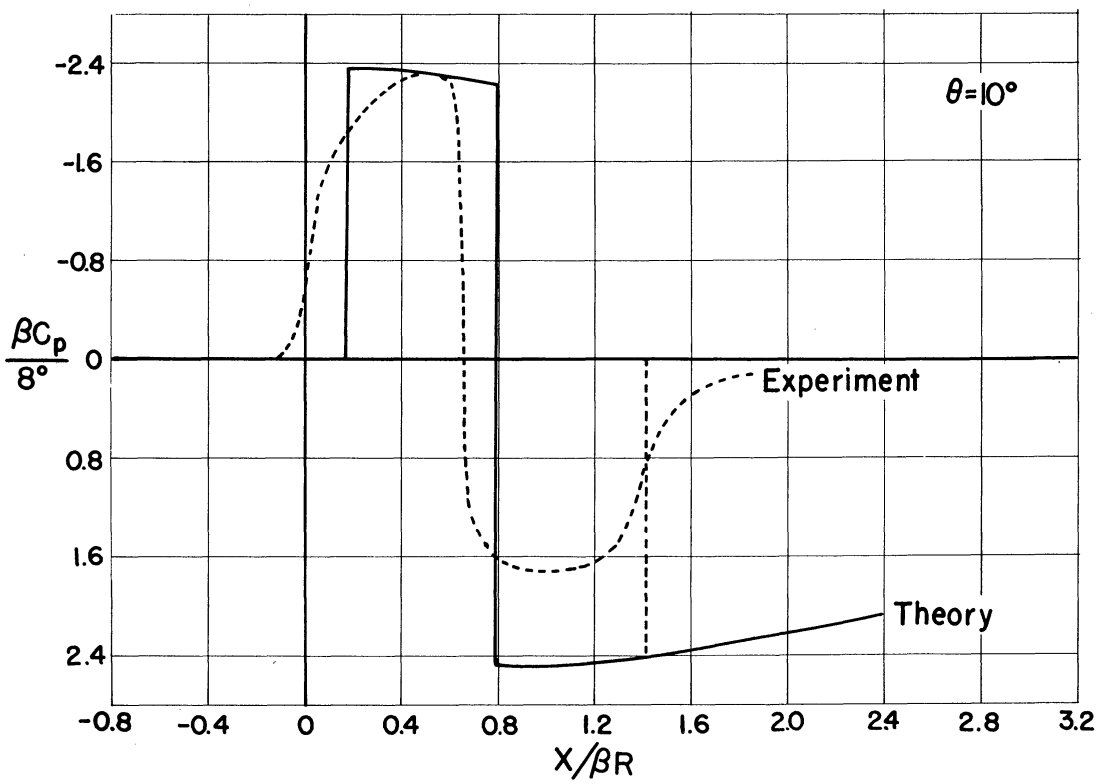

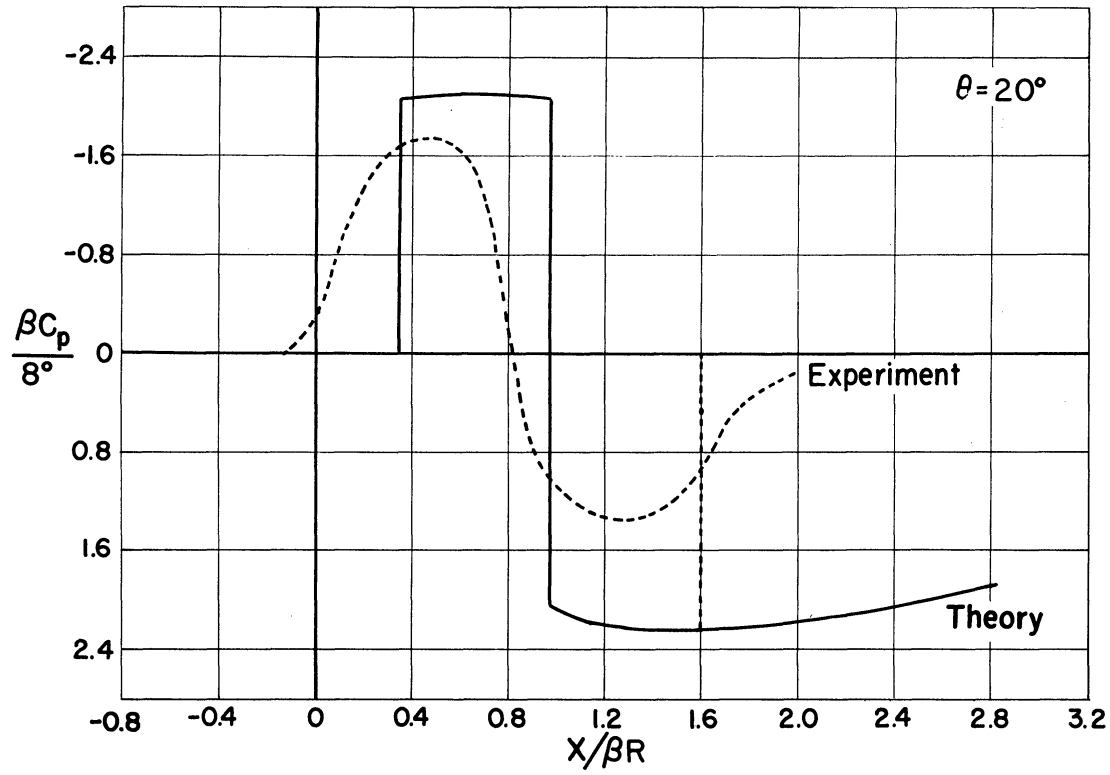

Fig. 11 — Pressure profiles: $\alpha_B = 0$, $\alpha_W = 0$, wedge surface of the wing

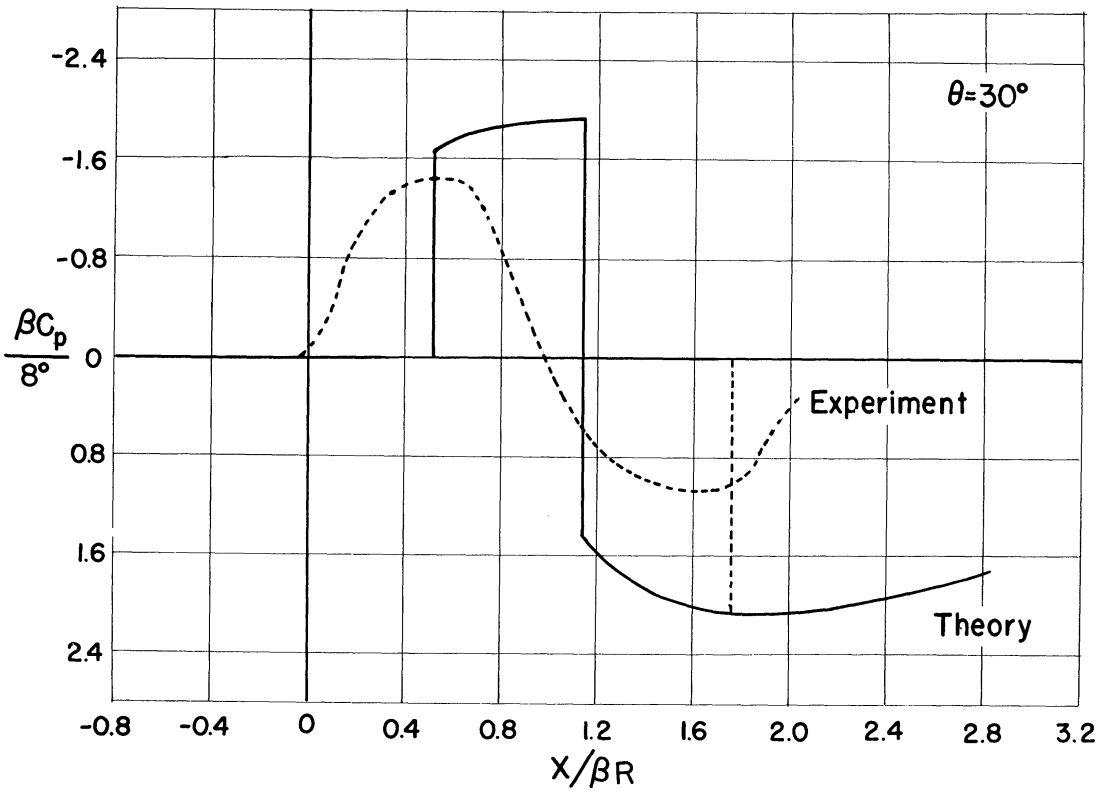

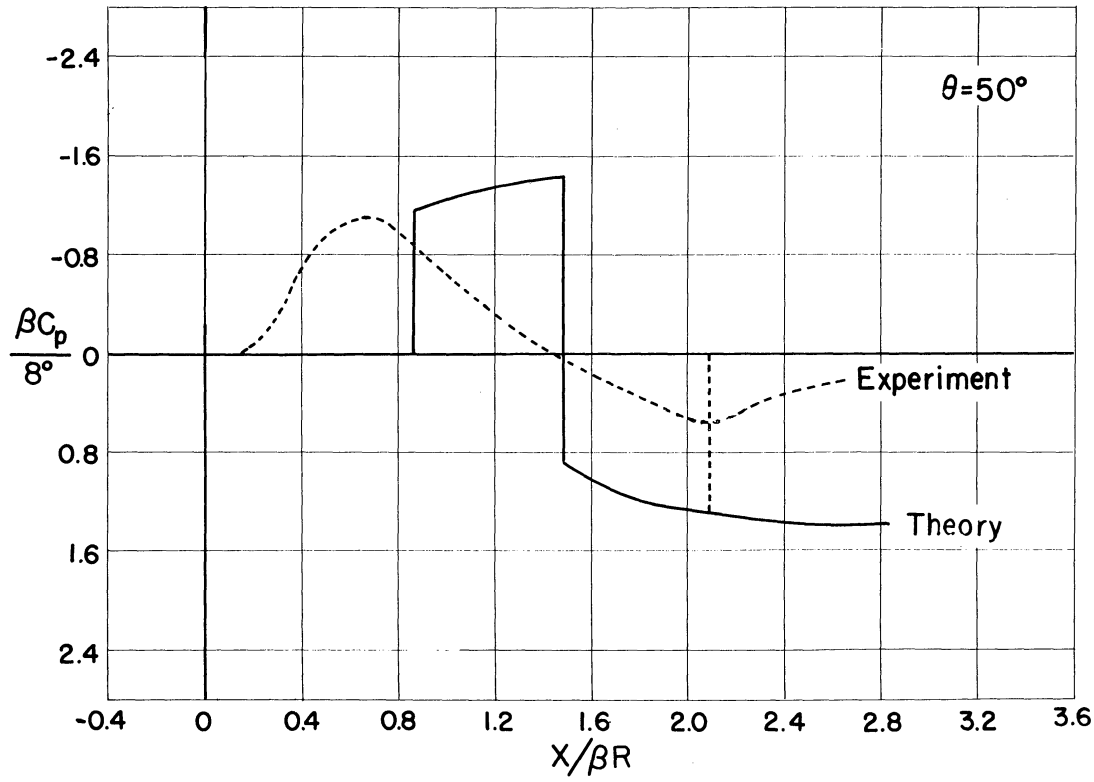

Fig. 11 (Continued)

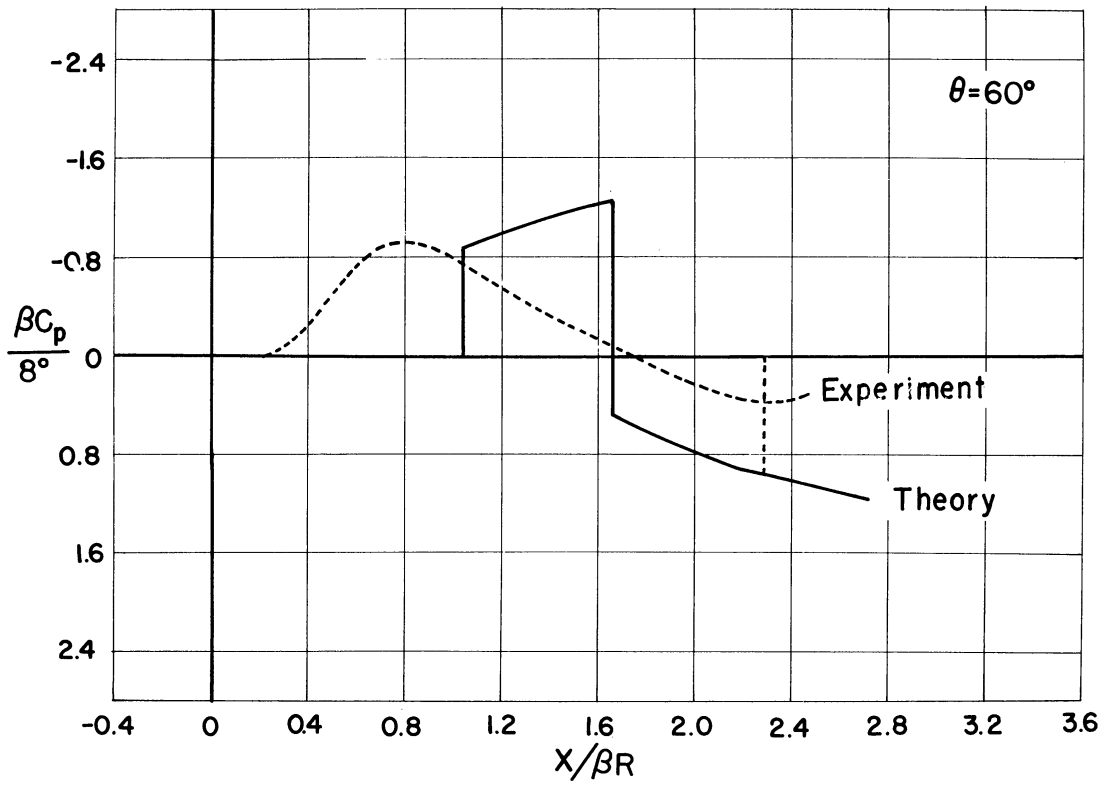

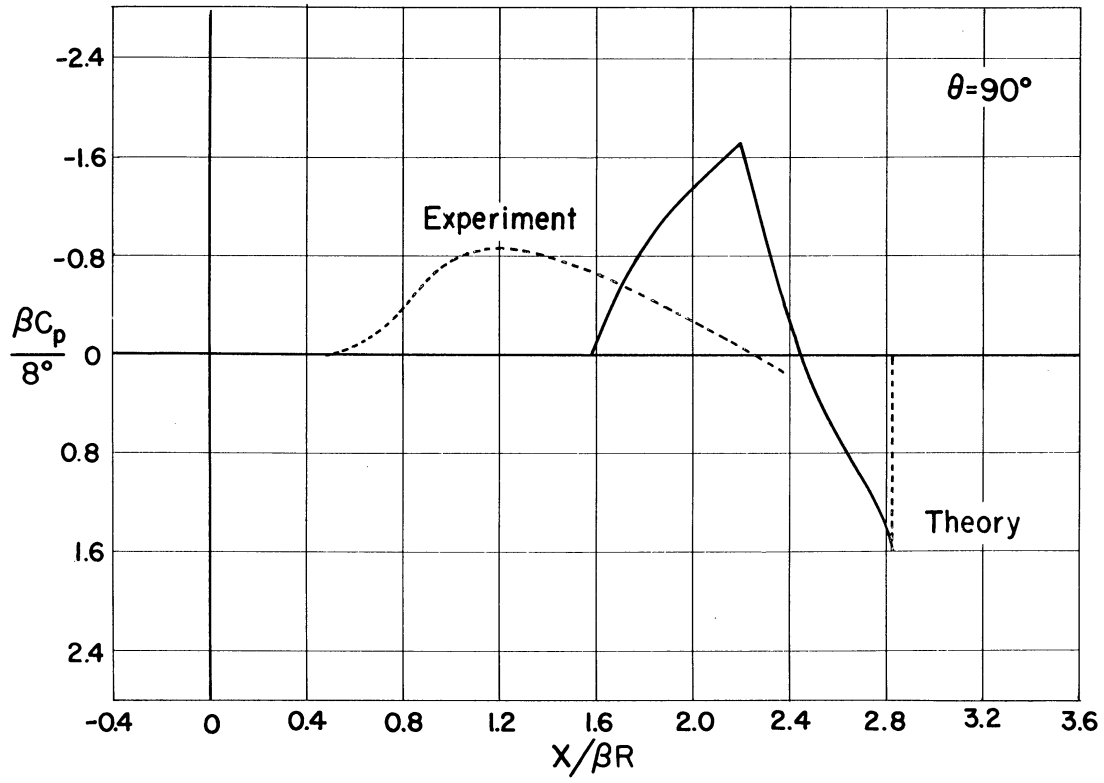

Fig. 11 (Concluded)

surface of the wing at -8° angle of attack. For the lower values of θ (i.e., $\theta < 30°$) the magnitude of the experimental pressure distributions agrees well with the values given by linearized theory over the front (compression) half of the wing chord, but falls short over the rear (expansion) half of the wing. This failure of the experimental curves to reach their theoretical values over the after portion of the wing is probably indicative of a separation at, or slightly to the rear of, the midchord point of the wing. China-clay patterns on the wedge surface of the wing also indicate that the flow is separated from the wing in this region.

The fact that the axial position at which the expansion should theoretically take place in the meridional plane $\theta = 10°$ is upstream of the axial position at which the experimental curves drop off sharply is in agreement with the traces in Fig. 5.

For larger values of θ the spreading out of this expansion wave as it progresses around the body results in an increasingly flatter slope of the pressure curves at the midchord point.

Figure 10, which is a composite of the pressure distributions for several values of θ when the wing is at +8° angle of attack, exhibits several interesting features. With this wing angle of attack the flow is deflected through an angle of 18° by an extremely strong shock wave at the wing leading edge. That this is an extremely strong shock wave is readily apparent from the fact that the maximum shock-wave deflection angle of Mach-number-1.9 flow is 23°.

This very strong pressure disturbance is propagated farther forward than for the shocks associated with smaller angles of attack. In the plane $\theta = -10°$ the disturbance is propagated approximately 4 boundary-layer thicknesses upstream, which increases to 11 boundary-layer thicknesses in the plane $\theta = -90°$.

The pressure profiles for $\theta = -10°$ and $\theta = -30°$ rise sharply to approximately one-half of the theoretical pressure rise, at which point there is a sharp, but small, decrease in pressure followed by a steep rise to the maximum pressure, which corresponds closely to the pressure rise through a shock wave giving an 18° deflection angle. For the higher values of θ this bump in the pressure profiles disappears and the curves rise to their maximum value monotonically.

An explanation of this double bump in the pressure profiles for the smaller values of θ may be deduced from the china-clay patterns on the body. Figure 12, as well as Fig. 8, show that two distinct lines originate close to the juncture of the body and the wing leading edge. These lines then diverge for increasing values of θ to form a triangular band with its apex at the juncture of the body and the wing leading edge. Inside this band the direction of the flow is in the direction of the shock traces, while behind the second line the flow has a component of velocity in the axial direction. It may well be

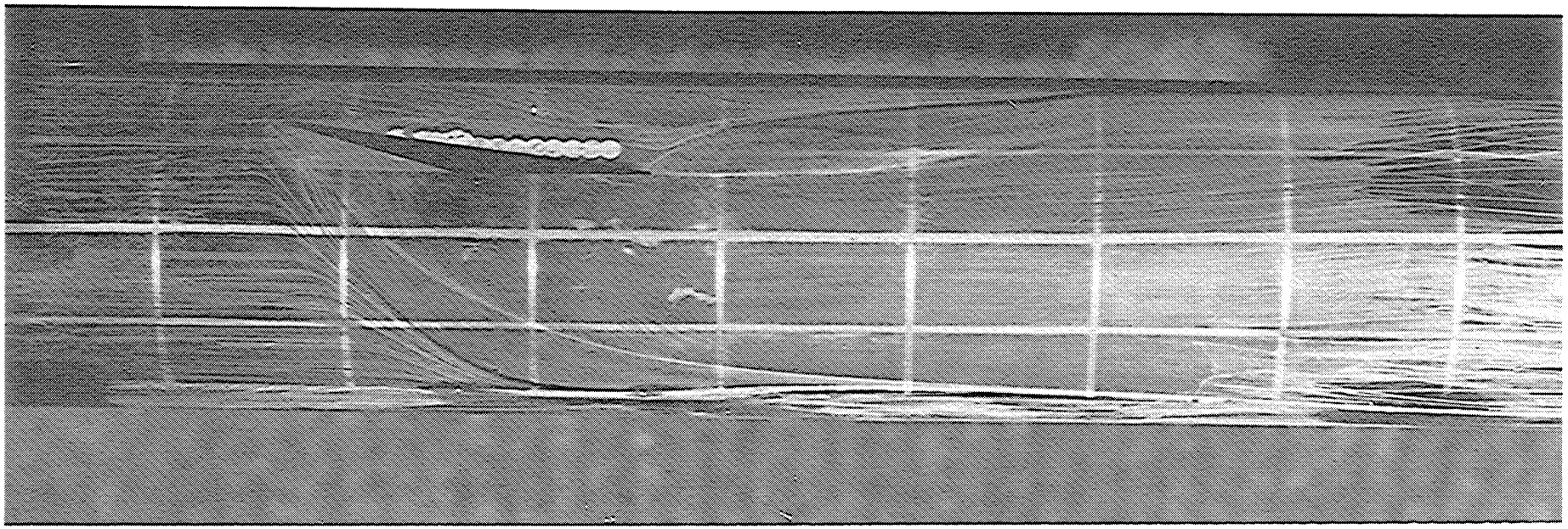

Fig. 12. China clay photograph: $\alpha_B = 0°, \alpha_W = +8°$.

that the very strong shock wave at the leading edge causes a local separation of the turbulent body boundary layer along the foremost line and a reattachment along the second line. In this way a separated channel is formed through which the slow-moving higher-pressure air flows radially out from and aft to the juncture region toward higher values of θ. The presence of such a bump in the boundary layer would account for the previously mentioned dips in the pressure profiles at the lower values of θ, since the bump would induce first a compression followed by a slight expansion as the air flows around the convex surface of the bump, and finally a second compression as the flow reattaches to the body surface. Just forward of the wing-body juncture the body boundary layer will increase in thickness because of the upstream propagation of the strong compression-shock disturbance. This in turn will cause deflection of the outer flow away from the body. Then as the air flows around the bump there will be a slight expansion, and finally the second compression caused by the reattachment of the boundary layer and a deflection of the stream downward by the wing surface itself.

The schlieren photograph, Fig. 13, indicates that for outboard wing positions the strong shock is attached to the wing leading edge. However, as the boundary layer flows out around the body toward the plane $\theta = -90°$ a wedge of slow-moving air causes a change in the effective body shape. Thus, in the plane $\theta = -90°$ there is a buildup of the boundary layer, which results in a series of compression Mach waves, which coalesce into a strong compression shock wave. The compression on the schlieren indicated by the first sharp line is the plane shock from the outboard sections of the wing. The envelope of the compressive Mach waves is clearly visible as the rear white line on the schlieren.

The pressure profiles for $\theta = -10°$ show that the expansion at the midchord point attains practically its full predicted value. This would indicate that the flow aft of the midchord point does not separate for this wing angle of attack as it does for 0 or $-8°$ angles of attack. This conclusion is verified by the china-clay pattern of the cambered side of the wing shown in Fig. 8. In addition, Fig. 8 indicates a strong flow from the wing onto the body ahead of the midchord point.

4. Effect of Variation in Boundary-Layer Thickness and Character

If the boundary-layer flow on the body is laminar, the experience obtained from the intersection of shock waves with laminar boundary layers over a flat plate[4] indicates that the upstream propagation of the disturbances due to shock waves originating at the wing edge will be increased. That this is indeed the case is borne out by the china-clay pattern shown in Fig. 14. The short body nosepiece was used in these tests in hopes of obtaining a laminar boundary layer on the body. Figure 14 shows that the laminar boundary layer probably separates

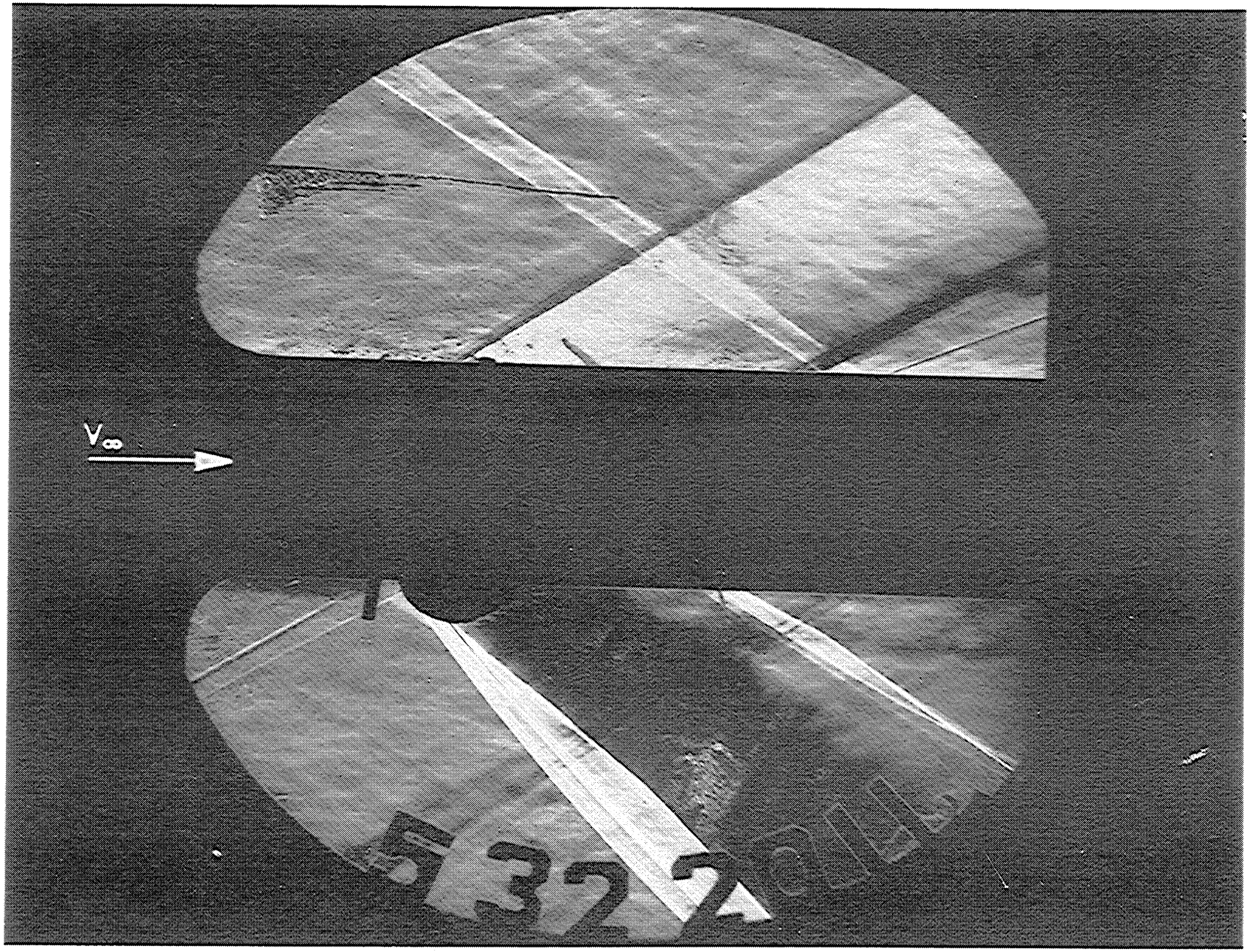

Fig. 13. Schlieren photograph : $\alpha_B = 0^\circ, \alpha_W = +8^\circ$

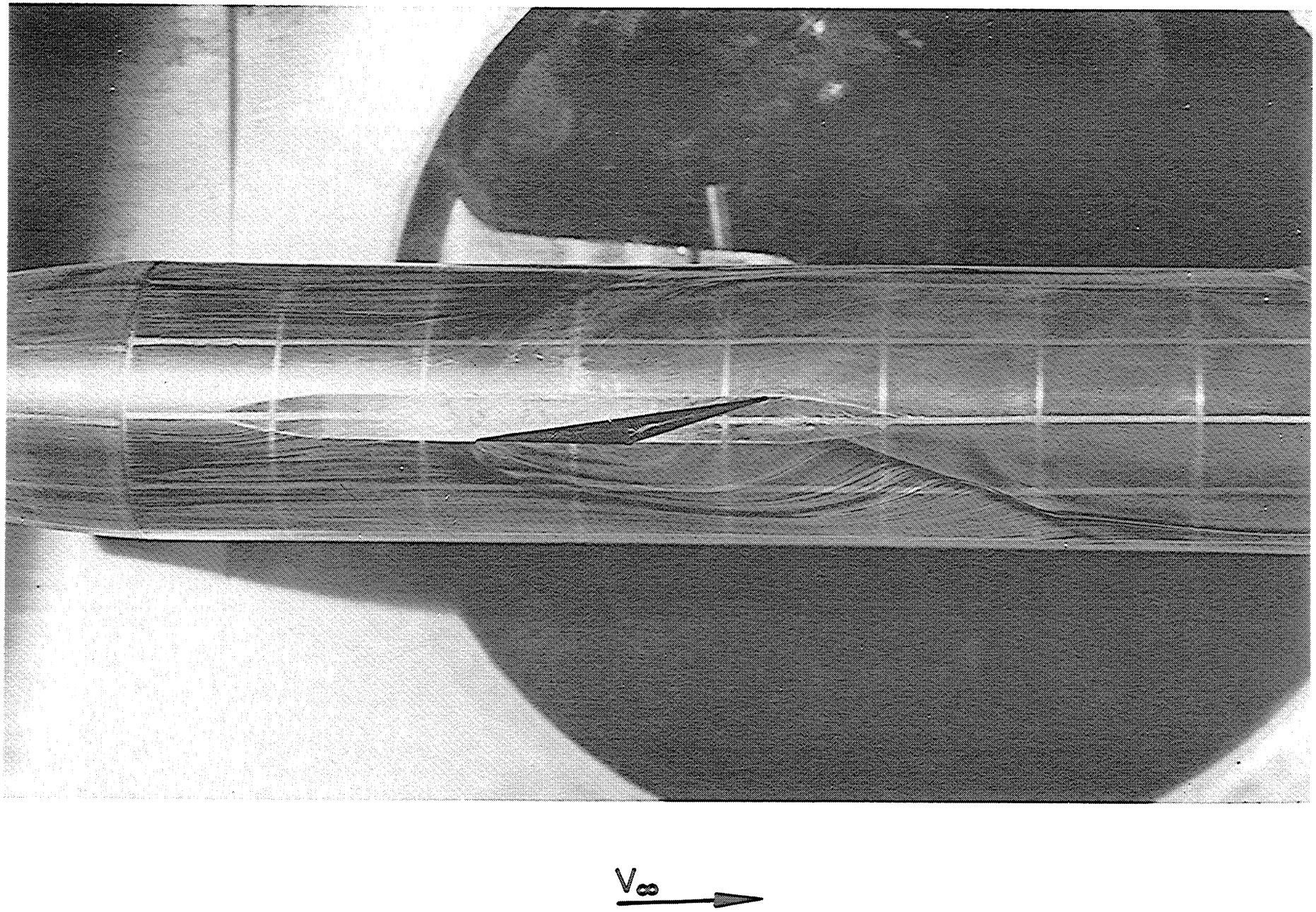

Fig. 14. China clay photograph: $\alpha_B = 0^\circ$, $\alpha_W = -8^\circ$, laminar boundary layer.

about 1 inch upstream of the Mach helix originating at the juncture of the wing leading edge and the body. A wide helical band around the body containing a strong boundary-layer crossflow is also visible. It may be conjectured from this picture that the wing leading-edge shock causes the laminar boundary layer on the body to separate well ahead of the actual intersection of this shock wave with the body, to form a channel through which the air in the boundary layer near the juncture flows toward the top of the body in much the same manner as that indicated in the previous section for the case of a very strong shock interacting with the turbulent boundary layer. No pressure distributions for laminar body boundary layer are available, since the body boundary layer was turbulent in the orifice region.

The transition distance for the body boundary layer varies with θ, occurring earlier for certain values of θ, probably because of small imperfections in the leading edge of the short nosepiece. On that side of the body which contained the pressure orifices, tests with the china-clay film indicated that a turbulent wedge of flow in the body boundary layer began about 1 inch aft of the nose and spread out through the meridional planes with increasing downstream distance, so that the pressure profiles obtained for this configuration are not characteristic of a laminar boundary layer on the body, but rather show the effect of a thinner turbulent boundary layer. This effect of a thinner turbulent boundary layer on the body pressure profiles is shown in Fig. 15, which contains the pressure profiles for the thin turbulent boundary layer and also those for the thicker turbulent boundary layer obtained for the same wing angle of attack but with the long body nosepiece and tripper wire. In addition, the linearized theoretical results of reference 1 are shown for comparison. From these pressure profiles it is apparent that the amount of upstream propagation of the leading-edge shock disturbance is diminished for the thinner turbulent boundary layer. No measurements of the boundary-layer thicknesses were available, so it is not possible to check whether the disturbance is propagated upstream the same number of boundary-layer thicknesses in each case. The shock jump is steeper and slightly higher for the thinner turbulent boundary layer.

In general, the pressures measured in the presence of a thinner turbulent boundary layer agree more closely with those predicted by the linear theory than do the pressures measured in the presence of a thicker turbulent boundary layer. However, if the boundary-layer flow over the body is laminar, the experimental pressure profiles may be considerably different from the values given by linearized theory.

5. Effect of a Gap between Wing and Body $\alpha_B = 0$ and $\alpha_W = -8°$

With the wings supported from the outboard tips (Fig. 1), it is possible to shift the wings outboard, and thus obtain an unobstructed gap between the

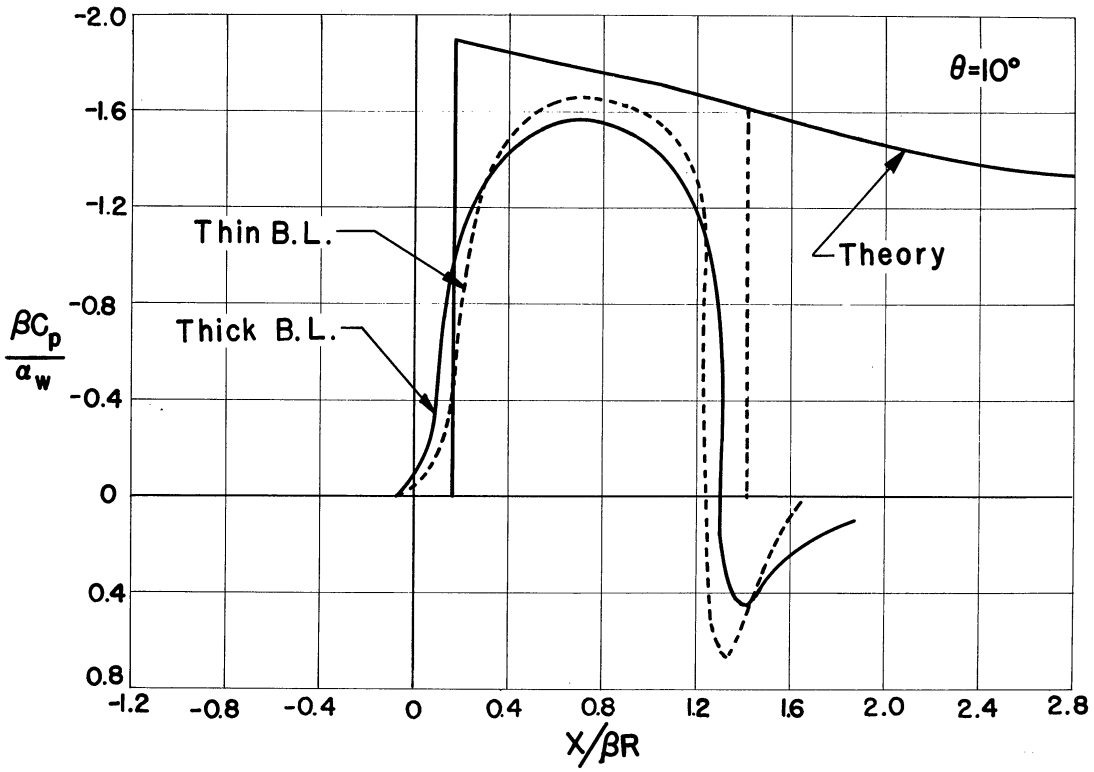

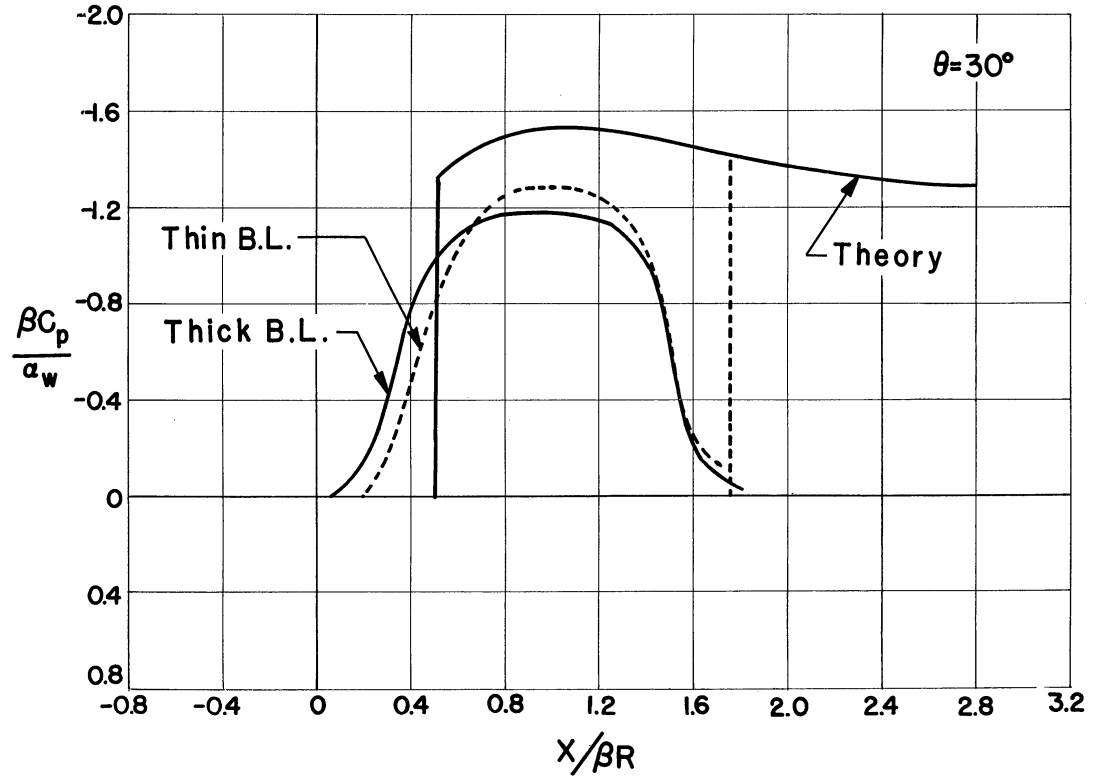

Fig. 15— Pressure profiles showing the effect of body boundary layer thickness, $\alpha_B = 0$, $\alpha_W = -8°$

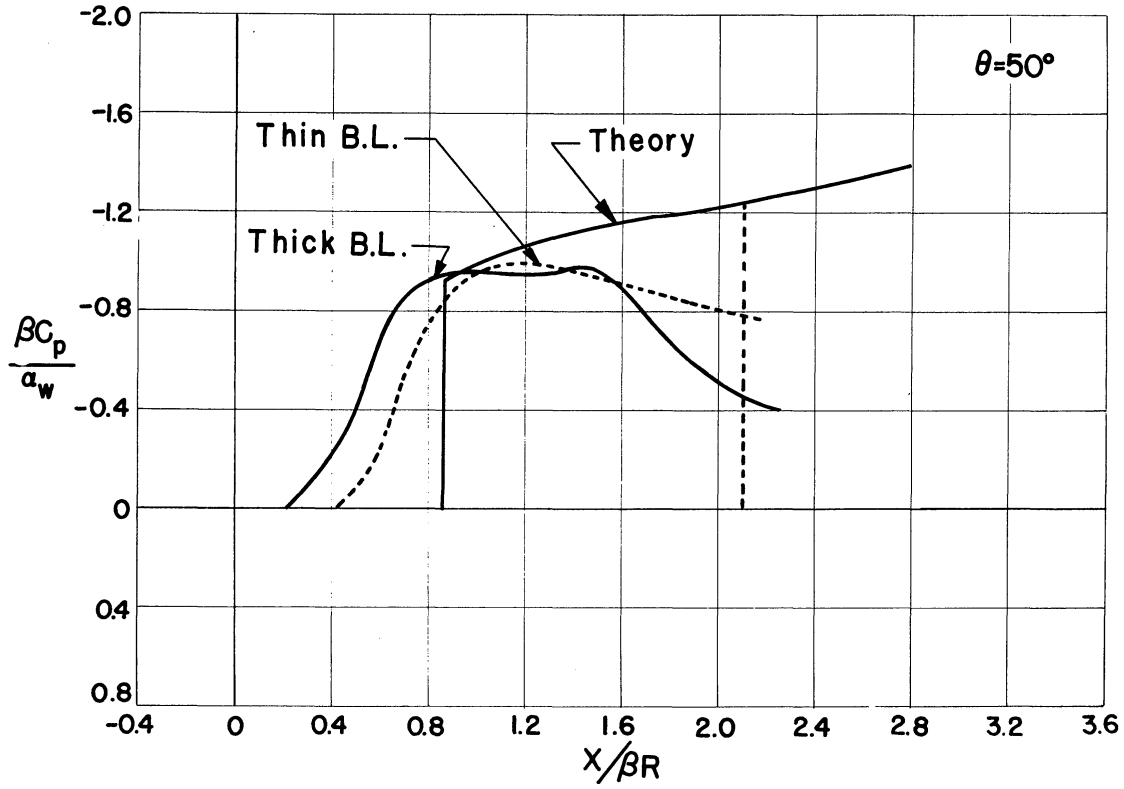

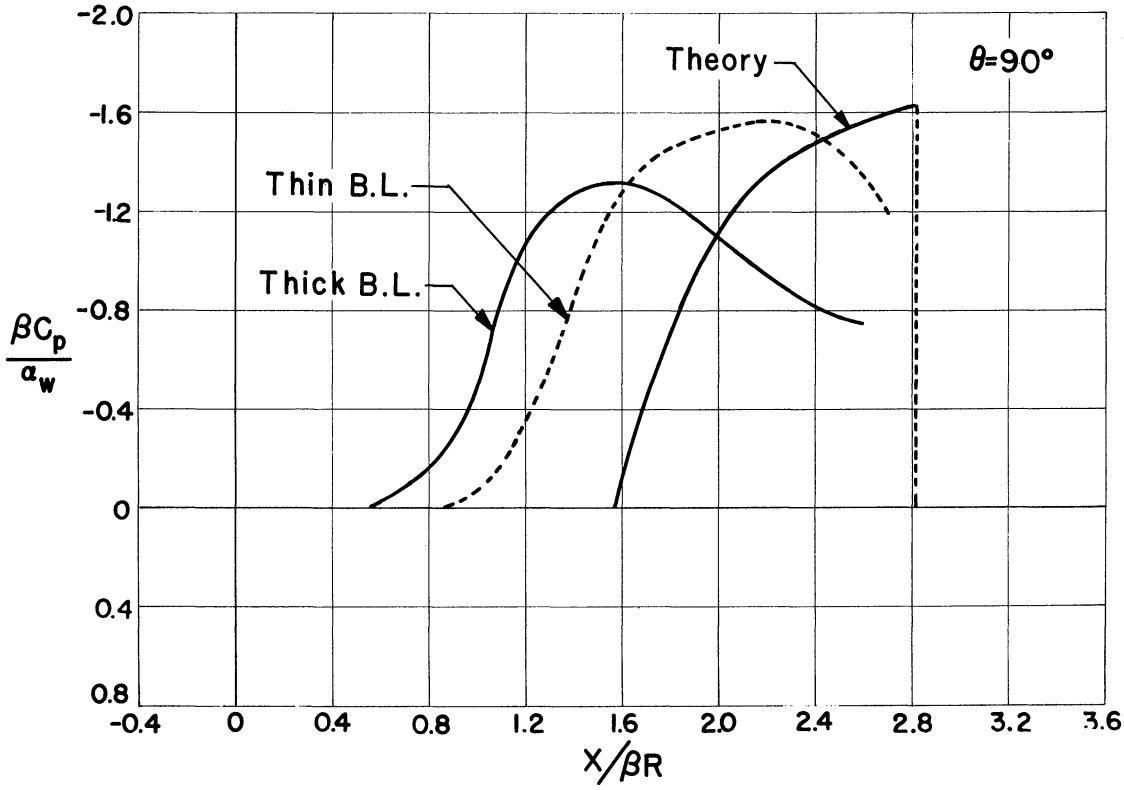

Fig. 15 (Concluded)

wing and the body. This gap will not be similar to the type of gap which would occur in a missile or aircraft in flight, since there is no structural connection between the wing and the body.

The pressure profiles which were recorded for a 0.10-inch gap and a 0.17-inch gap are shown in Fig. 16, where they may be compared to the pressure profiles obtained for the case of zero gap as well as the linearized theory results. For all curves in Fig. 16 $\alpha_B = 0°$ and $\alpha_w = -8°$.

The pressure curves indicate that in the plane $\theta = -90°$, i.e., on the bottom meridian which corresponds to the wedge surface of the wing, there is no appreciable effect due to gap. Even in the plane $\theta = -30°$ the effect of the gap is small. In the meridional plane $\theta = -10°$ the effect of the gap is small up to the midchord point, but aft of this point the effect of the gap seems to be to give pressure profiles which agree less well with the linearized theory for zero gap as the gap increases. This disagreement is attributed to the influx of the high-pressure air from the compression side of the wing into the low-pressure region aft of the midchord point.

On the part of the body associated with the flat surface of the wing the effect of the gap in the planes $\theta = +90°$ and $\theta = +30°$ is to reduce somewhat the peak pressures obtained. The pressure profiles in the meridional plane $\theta = +10°$ show similar effects up to the trailing edge, but aft of the trailing edge the over-expansion, which was mentioned earlier in the discussion of the pressure profiles for zero gap, increases markedly. This increase, however, seems to be the same regardless of the gap size. It is probable that the presence of a gap between wing and body is accompanied by a wing-tip vortex which affects the body pressure profiles more strongly closer to the wing plane.

Since the total body lift, drag, and moment coefficients would be obtained by an integration of the pressure profiles on the body, the effect of the gap on these quantities would not be large, since the area under each curve must be multiplied by $\sin\theta$, where θ is the meridional angle. Thus, while the presence of a gap between wing and body may alter the pressure profiles considerably in the immediate vicinity of the gap, the overall lift, drag, and moment of the body are probably relatively insensitive to the gap size.

Since no wing pressure distributions were obtained, it is not possible to make definite statements concerning the effect of wing-body gap on the wing lift, drag, and moment coefficients. However, it is likely that the wing pressure distribution is considerably altered by the presence of a gap which in effect will permit an equalization of pressure between the compression and expansion sides of the wing. Thus, the overall lift, drag, and moment coefficients of the body and wing in combination may be seriously affected by the presence of wing-body gap.

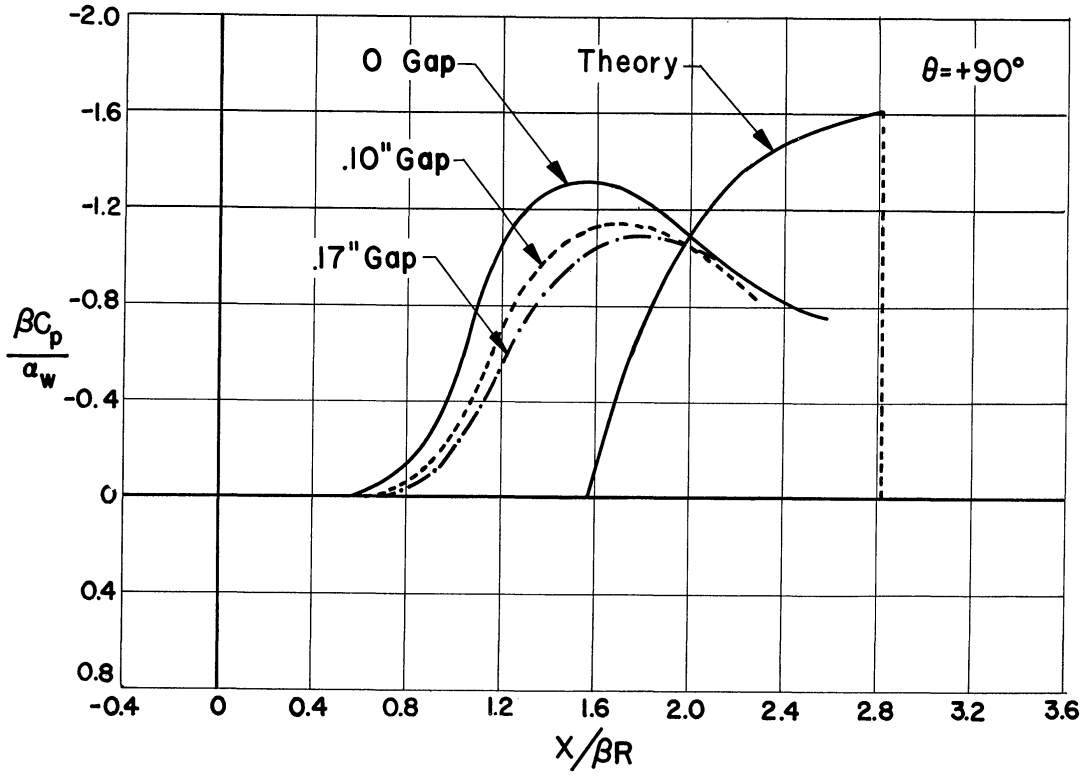

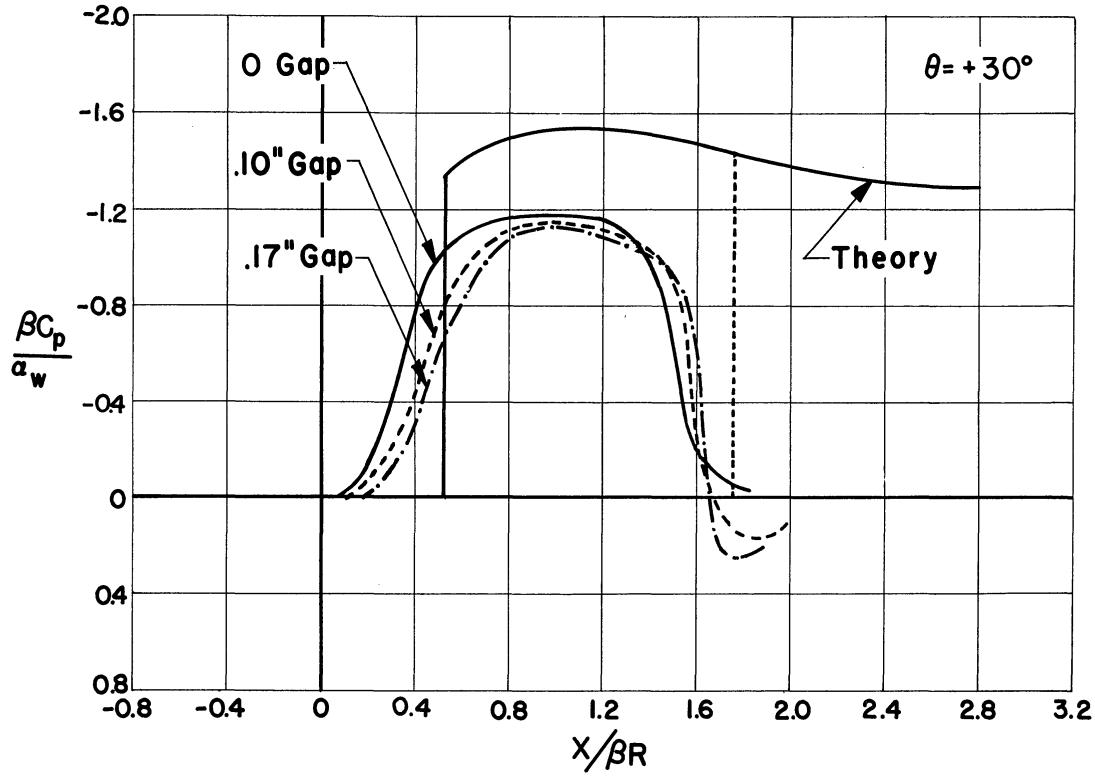

Fig. 16 — Pressure profiles showing effect of a gap between wing and body, $\alpha_B=0, \alpha_W=-8°$

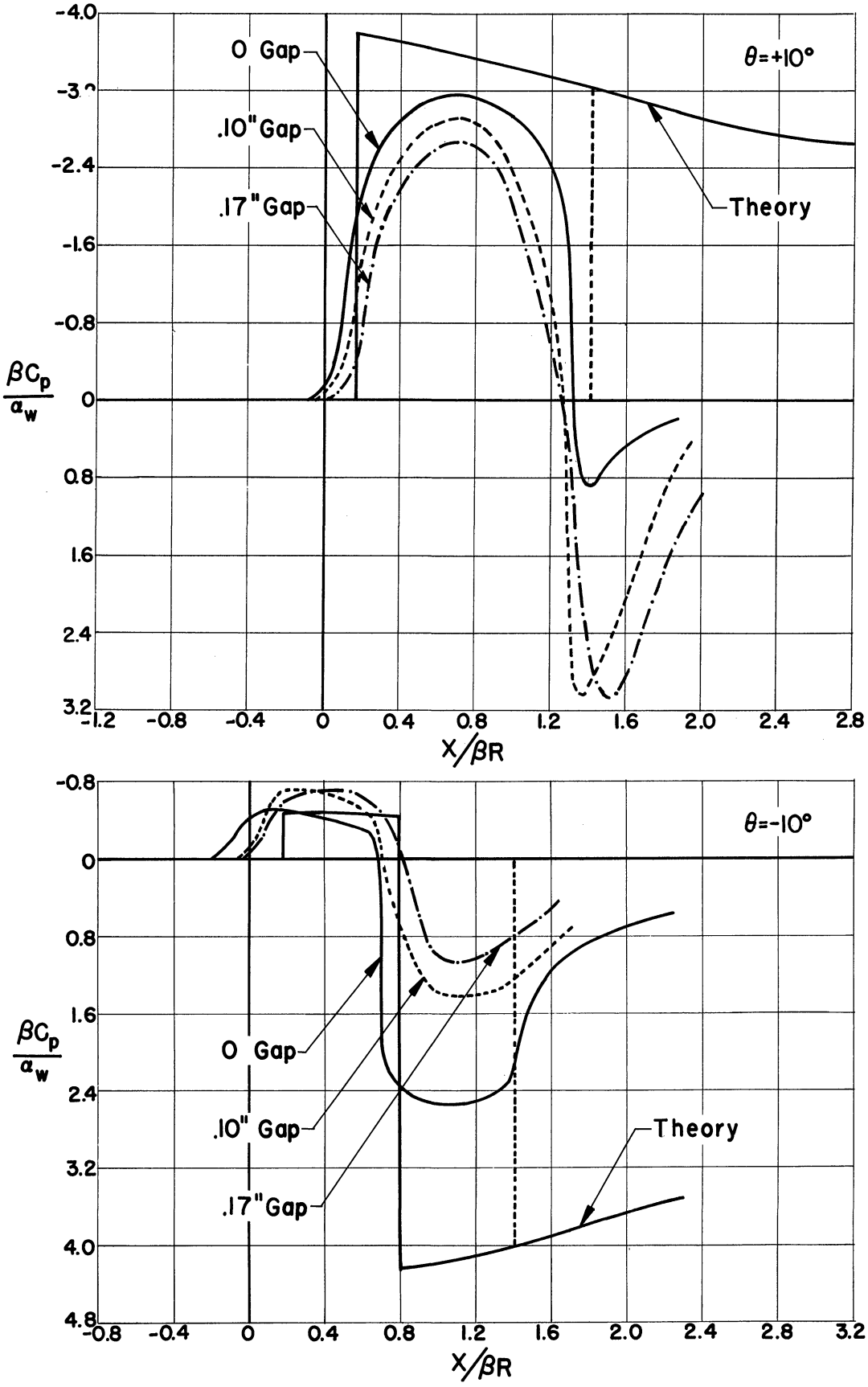

Fig. 16 (Continued)

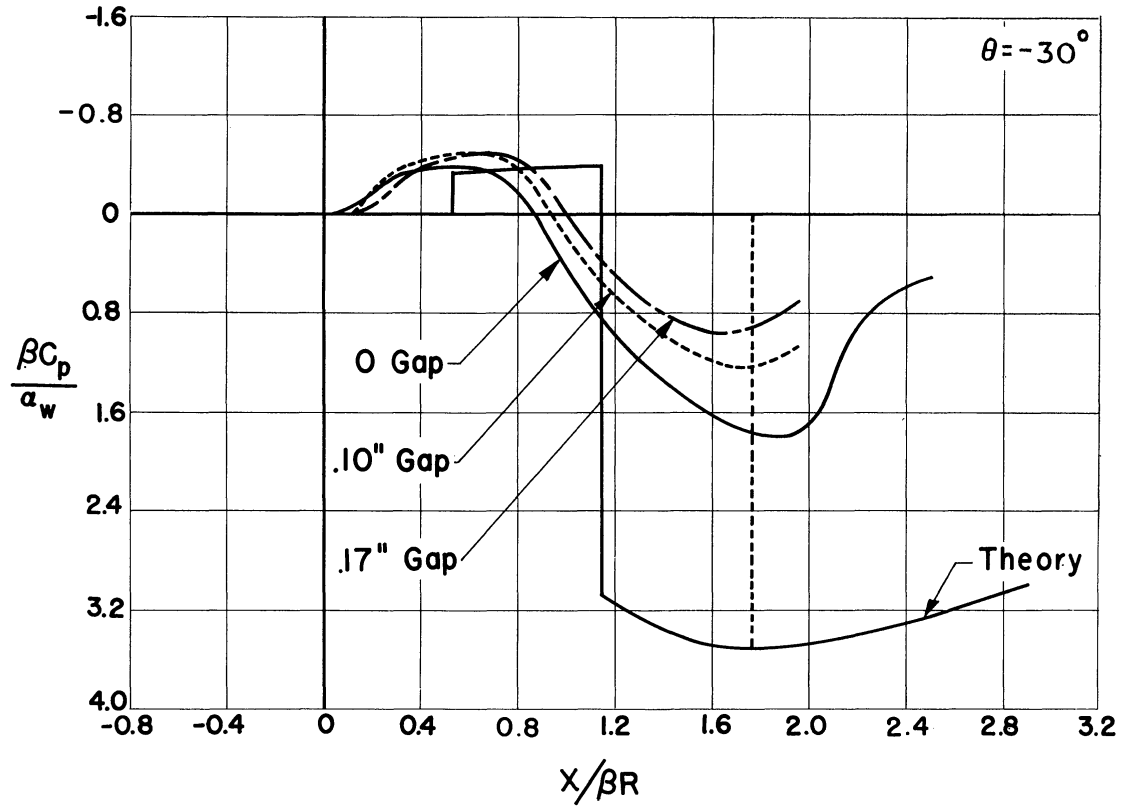

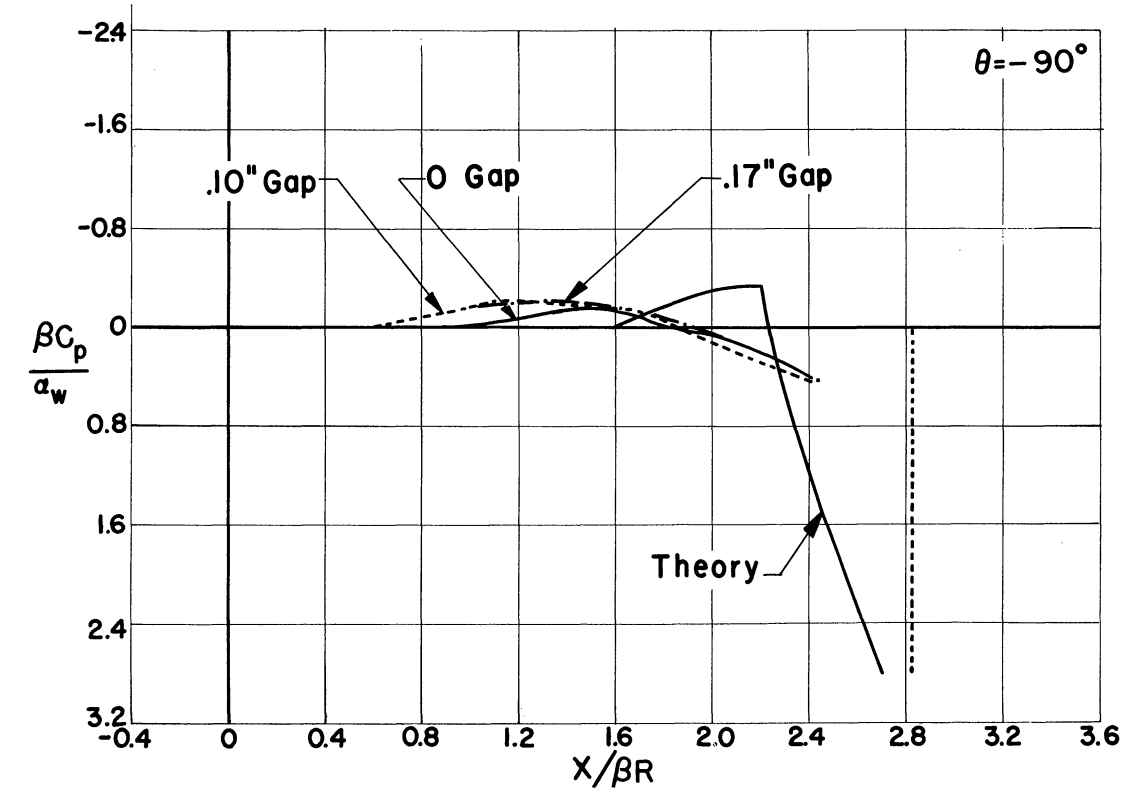

Fig. 16 (Concluded)

A comparison of Fig. 17, which shows the china-clay pattern on the body for the case of 0.17-inch gap between the wing and body, with Fig. 7 confirms the previously made statement, on the basis of the pressure distribution, that the effect of the wing leading-edge shock is weaker and there is an appreciable flow of air through the gap from the high-pressure region into the low-pressure region over the aft half of the wing. The flow over the body near the aft half of the wedge surface of the wing is more nearly in the free-stream direction for the case of 0.17-inch gap than it is for the case of zero gap.

China-clay patterns on the wedge surface of the wing in the gap case (Fig. 17) indicate separation of the flow at the midchord point just as in the zero-gap configuration. On the flat-surface (compression)side of the wing (Fig. 17) there is a definite indication that the high-pressure air flows inboard and then through the gap to the low-pressure side of the wing.

6. Body Alone at +8° Angle of Attack

For a right cylindrical body at an angle of attack in the uniform flow of an ideal fluid, the pressure distributions in planes normal to the body axis sufficiently far downstream of the body nose approach the doublet pressure distribution with a stagnation point on the lee side. There are, therefore, lateral potential gradients tending to promote crossflow away from the meridional plane $\theta = -90°$ and toward the meridional plane $\theta = +90°$.

H. J. Allen[14] has shown that a remarkable resemblance exists between the actual flow and pressure distributions in a normal plane at a distance x from the nose and the viscous flow around a two-dimensional cylinder at a time $t = x/V_\infty$ after having started from rest with a constant speed $V_n = V_\infty \sin \alpha_B$. Thus, the boundary-layer separation in two-dimensional flow corresponds to the rolling up of the vortices on the lee side of the body. The idealized doublet pressure distribution cannot be maintained and the pressure recovery on the lee side is incomplete. The overall lift and drag on the body are increased by the presence of the lee-side separation.

Both the pressure distribution (Fig. 18) and the china film pattern (Fig. 19) obtained in the present tests support the above picture. The experimental points shown in Fig. 18 are based on the average static pressures recorded from several runs of the body alone at angle of attack of +8° by the foremost plane of orifices. The dotted curve faired through these points represents the experimental pressure distribution on the body alone at angle of attack. It is apparent from Fig. 18 that the minimum pressure point on the body alone occurs for a value of θ slightly less than zero, and that the flow in the crossflow plane separates from the cylinder at around $\theta = +30°$. Actual mixing of the separated air with the mainstream air induces a flow of the separated air along the body axis in the mainstream direction. For values of θ lying between +30 and +90°, the pressure is roughly constant and slightly less than ambient pressure.

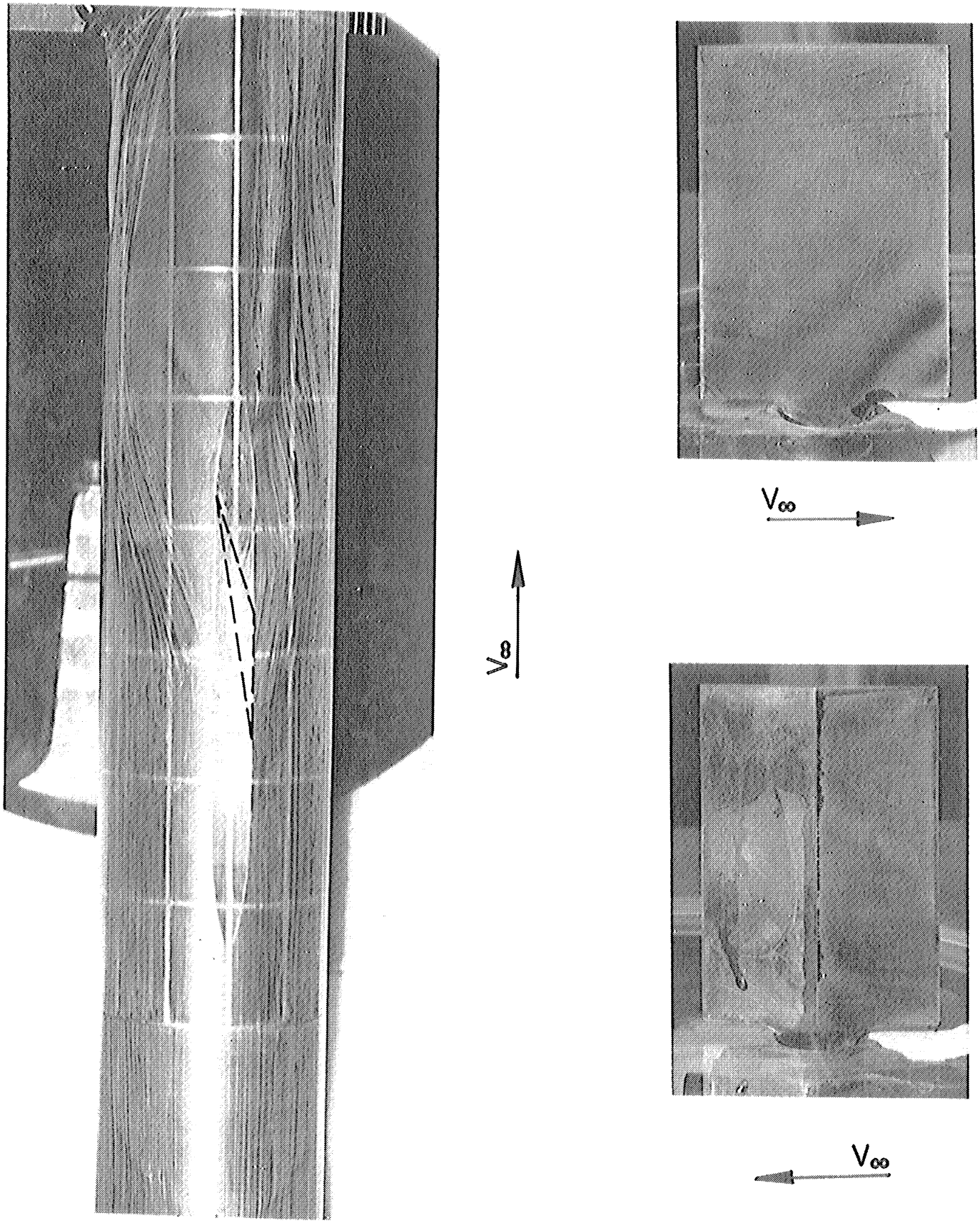

Fig.17. China clay photograph: $\alpha_B = 0^\circ, \alpha_W = -8^\circ$, gap = .17".

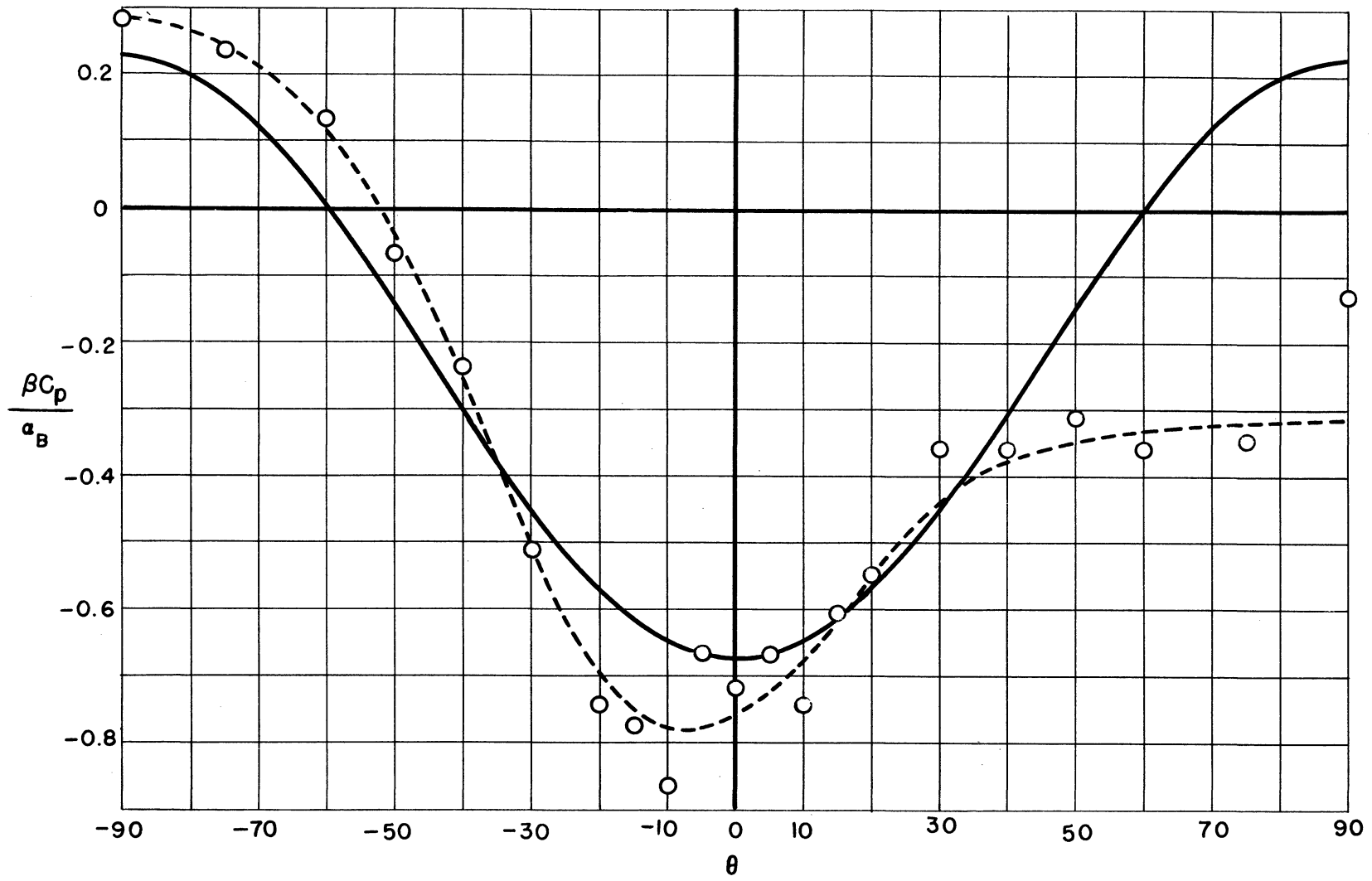

Fig. 18 — Pressure distribution on body alone at +8° angle of attack.

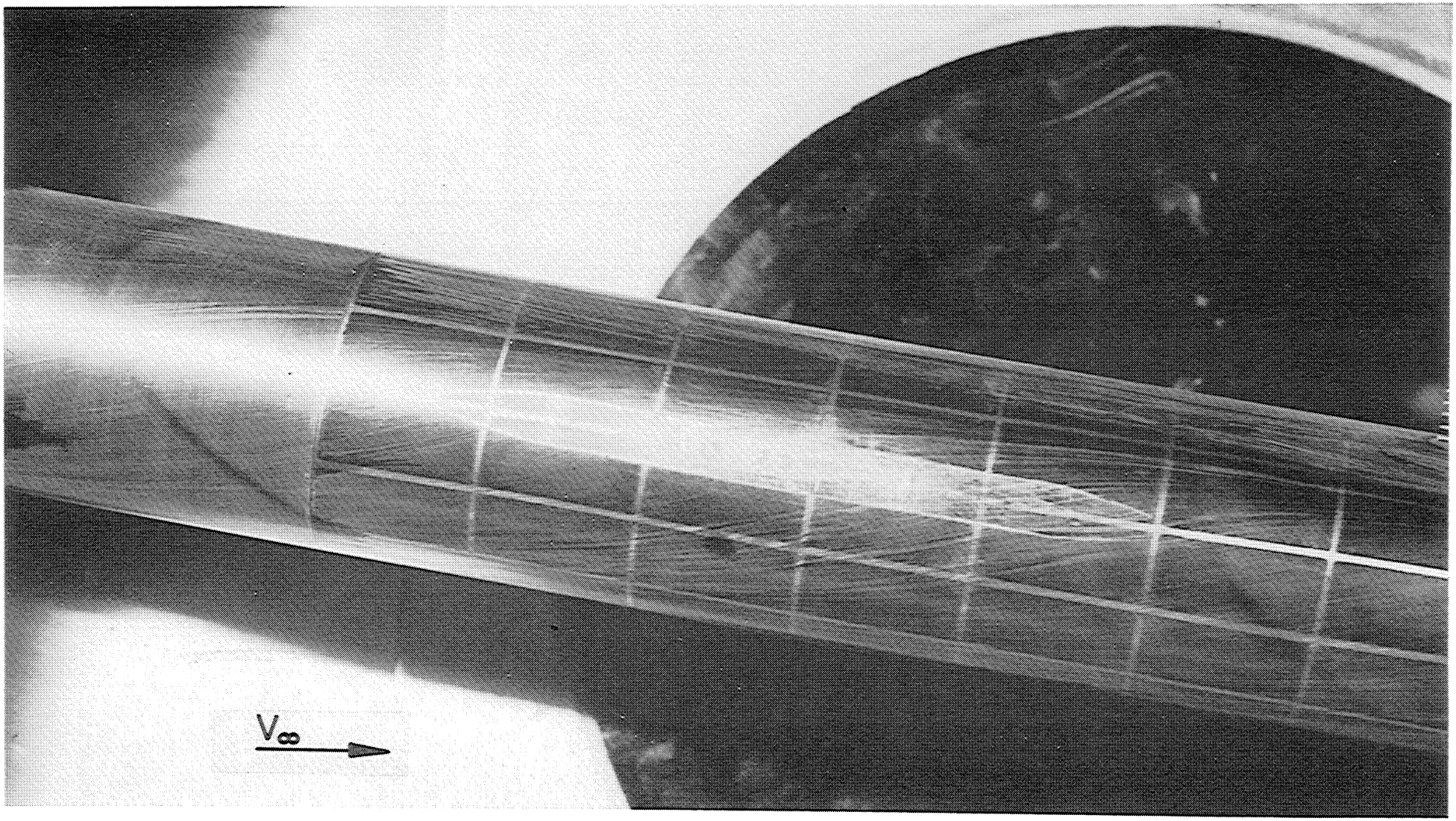

Fig. 19. China clay photograph: body alone, $\alpha_B = +8°$.

Measurements from Fig. 19 show that the flow near the surface in the boundary layer at $\theta = 0$ makes an angle of about 14° with the free-stream direction, which is 6° more than the 8° angle with respect to the free stream indicated by the theoretical doublet crossflow. On the lee side of the body this angle rapidly decreases with increasing θ until at $\theta = 30°$ the flow is in the direction of the body axis. For the top meridional planes, i.e., θ near 90°, the flow direction actually reverses and there is a tendency for the air to flow away from the 90° meridian toward the separation point.

Figure 20 is a schlieren photograph of the flow about the body alone at an 8° angle of attack. The boundary-layer thickness in the meridian plane $\theta = -90°$, as measured in the schlieren photograph, is 0.08 to 0.10 inch as compared to the 0.20-inch boundary-layer thickness for the body at zero angle of attack. On the lee side of the body in the plane $\theta = +90°$ the boundary layer appears to be separated. The disturbance waves, which are generated at the body nose and the roughness ring, curve forward slightly as they enter the separated region due to the fact that the velocities in this region are lower than the free-stream velocity. It should be remembered that the schlieren photograph gives a superposed series of two-dimensional pheonomena. For this reason the shock waves in Fig. 20 appear to split as they enter the separated region. The foremost leg of each of these waves represents the trace of the shock wave in the separated region, while the rear leg of each wave represents that portion of the wave which is in the outer unseparated flow. The outer edge of the separated flow is not clearly discernible in Fig. 20; however, the splitting of the shock waves as they enter the separated region occurs at about 1.2 inches from the cylindrical surface. This does not mean that the separated region is 1.2 inches thick on the lee side of the body, however, since some bending of shock waves entering the region is to be expected even in the absence of viscosity and separation due to the doublet potential flow in planes perpendicular to the body axis. The presence of this separated region on the lee side of the body will of course materially affect the interference pressure profiles obtained when the wing abuts the cylindrical body at an angle of attack.

As mentioned in section C,5, the measured pressure may be expressed as

$$p_{measured} = p_{body\ alone} + \Delta p_{induced} .$$

However, unlike the case of the body at zero angle of attack, the value of $p_{body\ alone}$ will no longer be constant for all values of θ. In addition to the variation of $p_{body\ alone}$ with θ, there will be some variation of $p_{body\ alone}$ with the axial distance x. This variation with x results from the finite distance between the nose and the point at which the static pressures are measured. In other words, the application of the local sweep-back principle is strictly valid only for a cylinder of infinite length, and the pressures measured in the present case still contain some of the transient effect due to the finite distance between the nose and the pressure orifices.

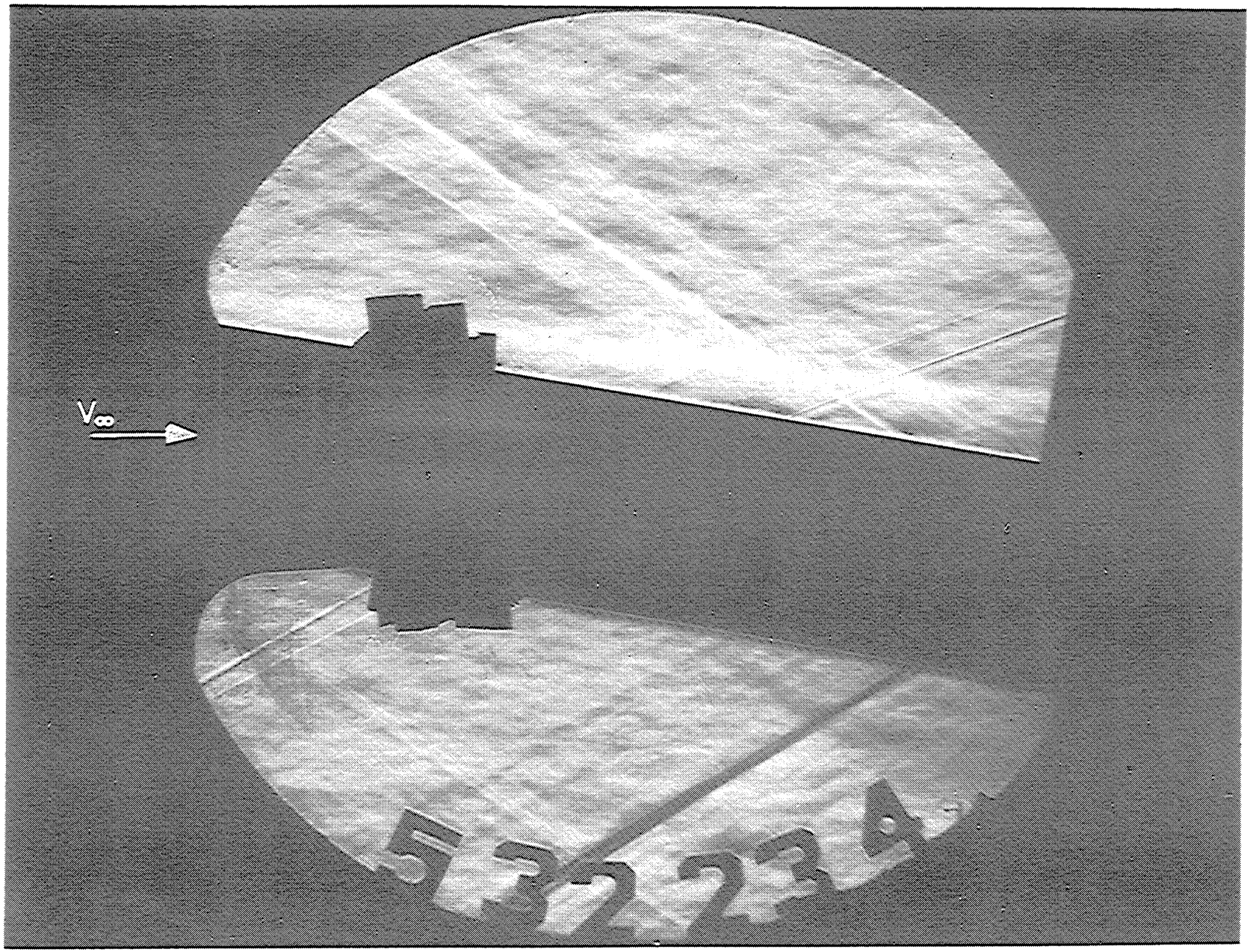

Fig. 20. Schlieren photograph: body alone, $\alpha_B = +8^\circ$.

The result of this body field is to make orifices located further from the nose read constantly higher values of static pressure. Thus, instead of a continuous pressure profile being traced out by the row of orifices in any one meridional plane, the pressure profile will consist of segments of the pressure profile with a step discontinuity in pressure between each segment. In fairing the experimental data, it is convenient to shift the rear segments of these curves downward to obtain continuous pressure profiles. No additional error will be introduced in the interference pressure distributions as long as the segments of the pressure profiles for the body alone are shifted by the same amount as the segments of the pressure profiles for body and wing.

7. Body at +8° Angle of Attack with Flat Surface of the Wing at Zero Angle of Attack

Figure 21 shows the theoretical pressure profiles, which were computed as outlined in reference 16, and the experimental pressure profiles on both the incident and the lee side of the body. Pressure profiles for the meridional planes $\theta = \pm 10$, ± 30, ± 50, and $\pm 90°$ are presented. The curves are plots of $\beta C_p / \alpha_B$ vs. x/β. All the experimental pressure profiles for the body at angle of attack have been shifted slightly so that the pressure on the body ahead of the wing agrees with the pressure represented by the dotted line in Fig. 18. Thus, the vertical displacement of the horizontal dotted line from the solid horizontal line may be traced to the flow separation on the lee side of the body. The actual amount of the vertical shift is easily obtained from Fig. 18. The pressure profiles are presented with the faired experimental curve of Fig. 18 as a base from which the interference pressures are measured, since the difference between the pressures for the body alone and the body with wing are more accurate than the absolute values of the static pressures measured on the body alone.

The pressure profiles indicate that if the point at which linearized theory predicts the first interference effects is shifted to the position at which an exact theory must predict the first interference effects (see Fig. 5), then the upstream propagation of the pressure disturbances on the incident side of the body is about 2 boundary-layer thicknesses for all values of θ where the boundary-layer thickness is taken to be 0.20 inch, the same as for the body at zero angle of attack. Actually, as mentioned in the previous discussion of the flow about the body alone at angle of attack, schlieren photographs show that the boundary-layer thickness in the meridional plane $\theta = -90°$ is about 0.10 inch and varies with θ until separation occurs at $\theta = +30°$.

On the lee side of the body the upstream propagation of the pressure disturbance varies from about 3 boundary-layer thicknesses in the plane $\theta = +10°$ to about 6 boundary-layer thicknesses in the plane $\theta = +90°$. The disturbance generated at the wing leading edge on the lee side will be an expansion wave

which deflects the flow near the body through about 8°, and this deflection angle dies out along the span inversely as the square of the distance from the body axis.

In general, Fig. 21 shows that the pressure rise on the incident side of the body falls somewhat short of the values predicted by linearized theory, although the agreement between theory and experiment seems to improve near the wing trailing edge. The very sharp spikes predicted near the wing leading edge seem to be considerably smoothed out by the body boundary layer.

On the lee side of the body the experimental pressures seem to be somewhat lower than those predicted by theory, although the sharp drops in pressure at the wing leading edge are softened by the effect of the body boundary layer. The pressure profiles for the meridional planes θ = +10 and +30° indicate the presence of a very weak compression shock prior to the expansion, which originates at the wing leading edge on the lee side of the body. The presence of this weak compression is confirmed by the china-clay patterns observed for this configuration.

Both the pressure profiles in Fig. 21 and the china-clay patterns indicate that aft of the wing trailing edge the flow tends to return to the flow about a cylinder at angle of attack. Flow patterns observed on the incident face of the wing indicate a uniform flow over the wing with no flow of the boundary layer onto the body from the wing. On the other hand, the china-clay patterns on the lee side of the wing show that the flow on the wing is toward the body.

8. Body and Flat Surface of the Wing at +8° Angle of Attack

The experimental pressure profiles for this configuration are presented in Fig. 22 for meridional angles of $\theta = \pm 10, \pm 30, \pm 50$, and $\pm 90°$, together with the linearized theory pressure profiles obtained by combining the linearized solution of the previous configuration with the linearized solution presented in reference 1. The upstream propagation of the expansion wave originating at the wing leading edge, which in this case must deflect the flow near the body through an angle of +16° on the lee side of the body, varies from about 3 boundary-layer thicknesses in the plane θ = +10° to about 6 boundary-layer thicknesses at the top meridian plane θ = +90°. This is the same variation as that observed for the previous configuration in which the wing angle of attack was zero.

On the incident side of the body the upstream propagation of the leading-edge shock wave, which must deflect the flow near the body through an angle of 16°, varies from about 2 boundary-layer thicknesses in the plane θ = -10° to about 5 boundary-layer thicknesses in the plane θ = -90°.

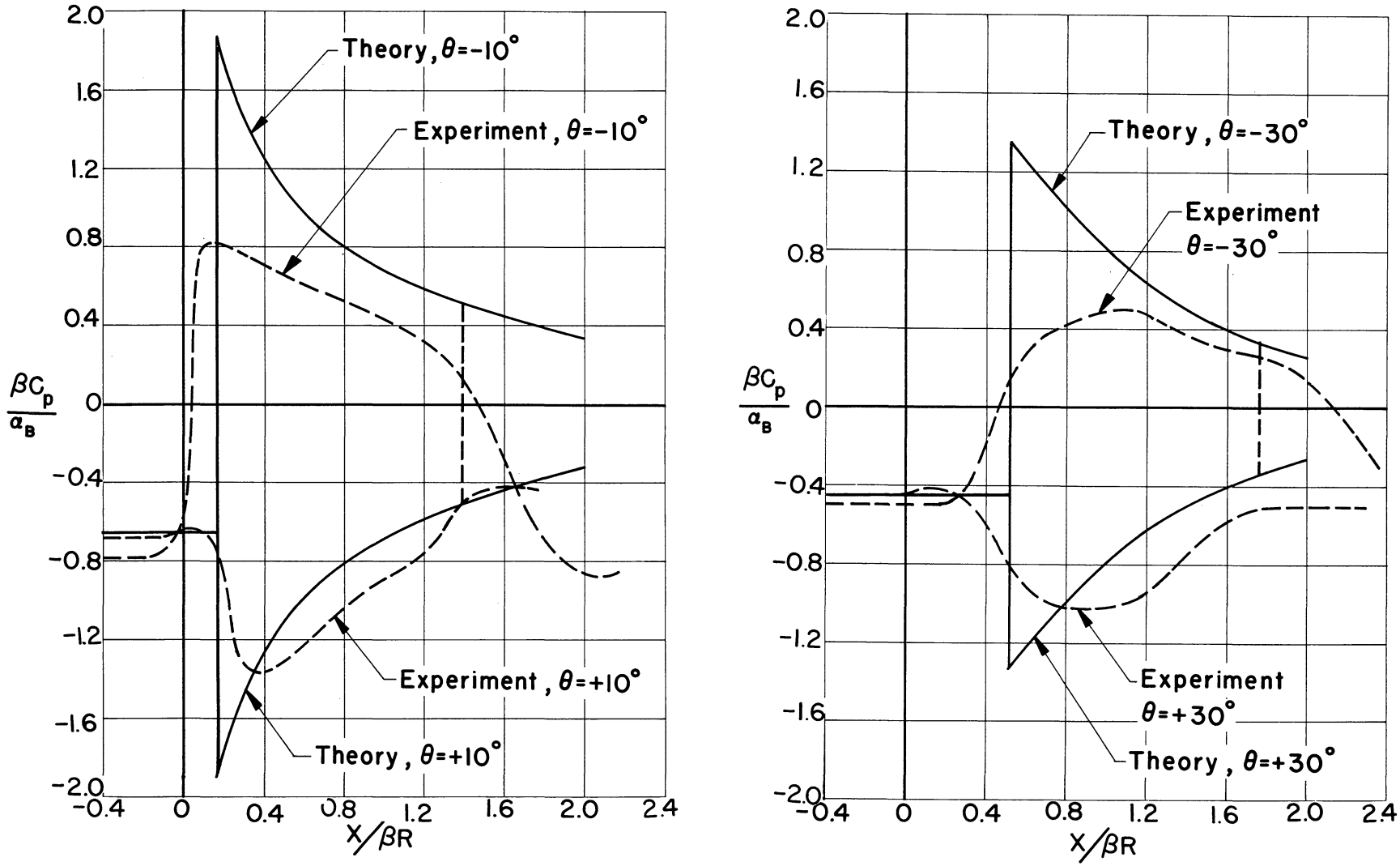

Fig. 21–Pressure profiles: α_B=+8°, α_W=0, flat surface of the wing.

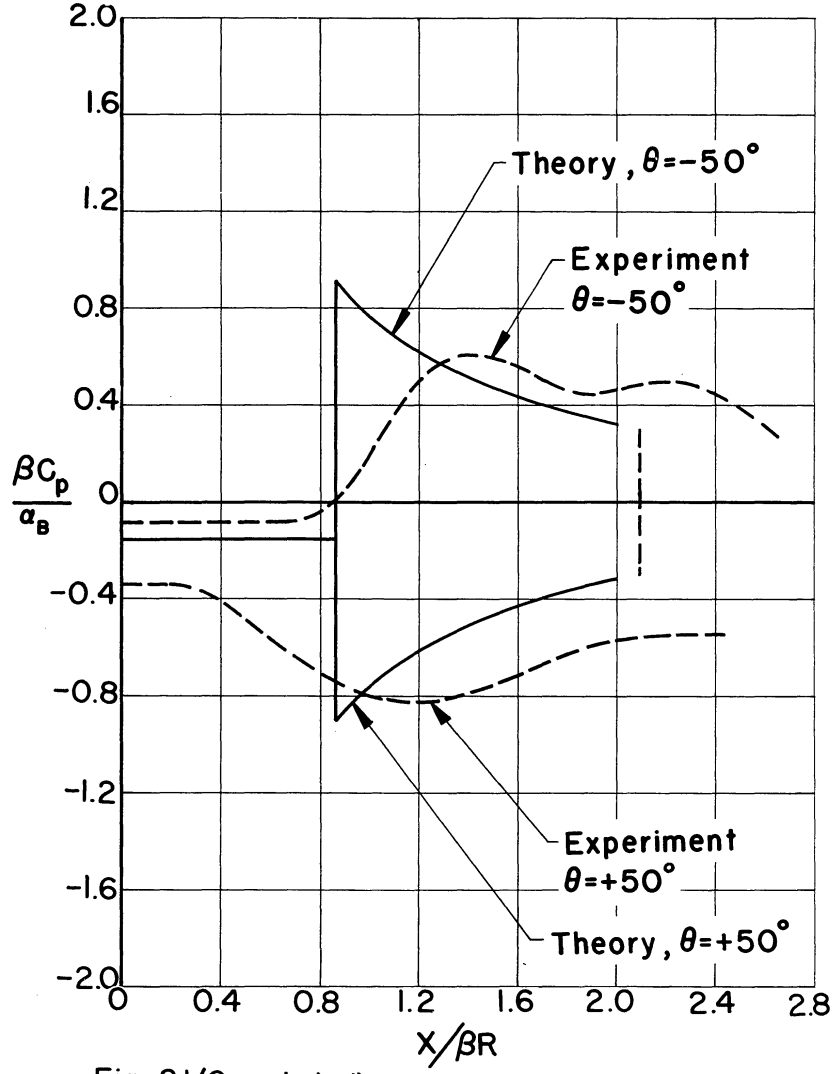

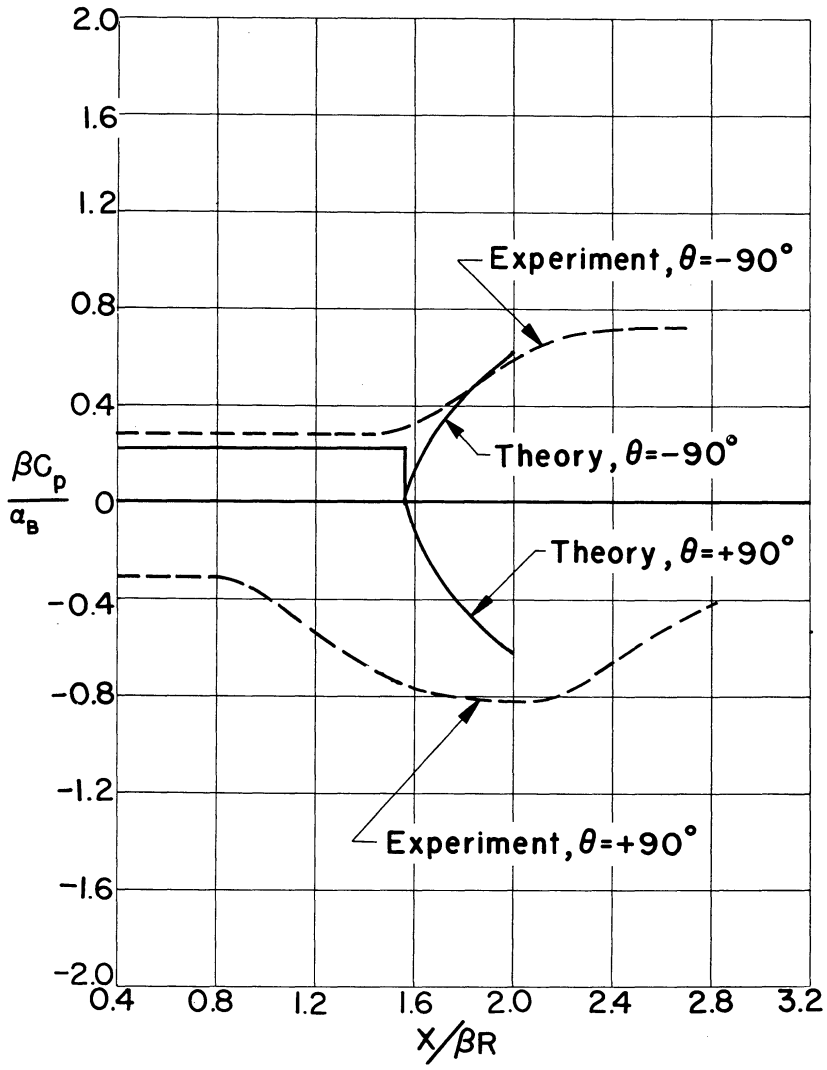

Fig. 21 (Concluded)

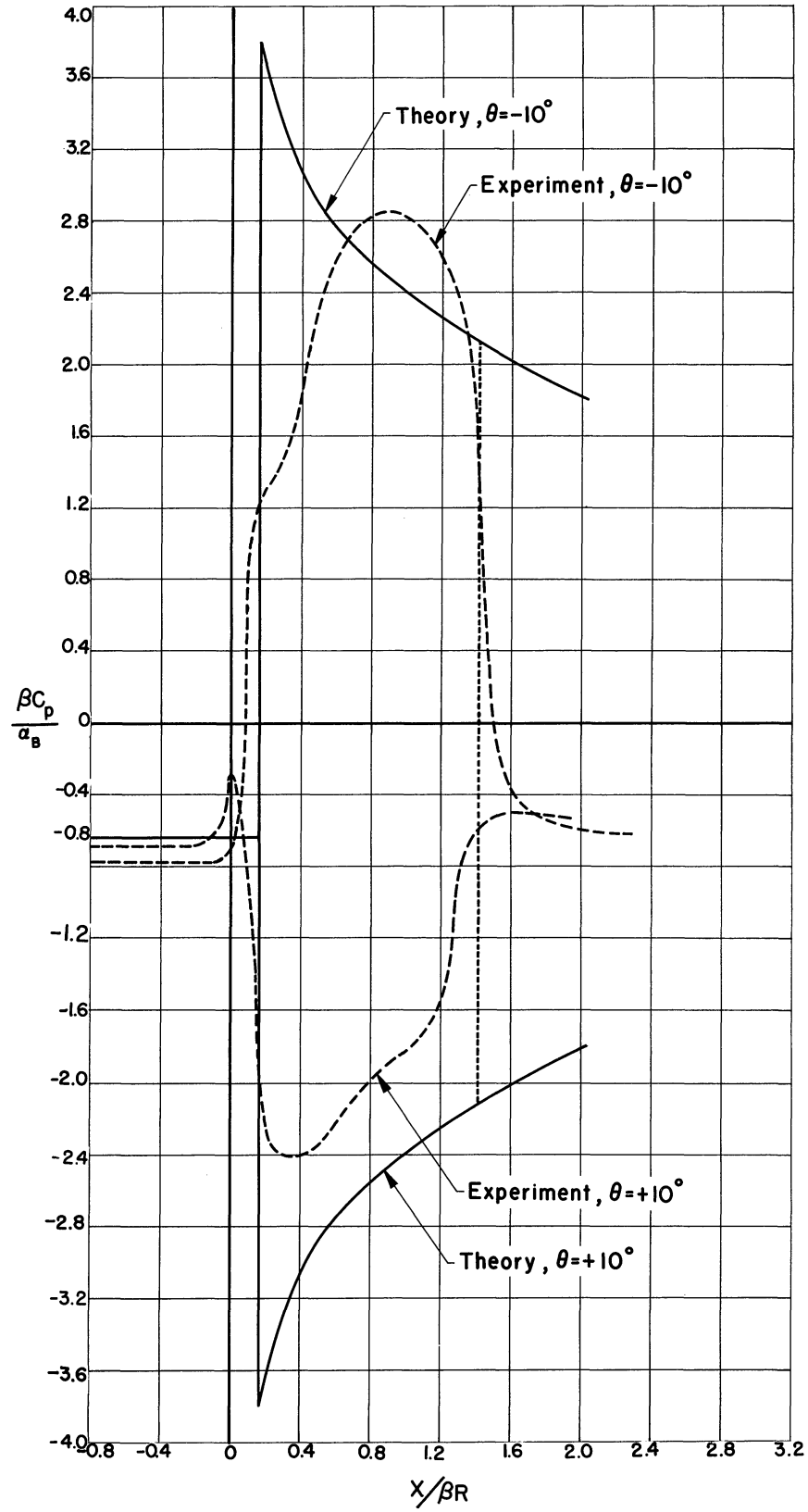

Fig. 22—Pressure profiles: $\alpha_B = +8°$, $\alpha_W = +8°$, flat surface of the wing.

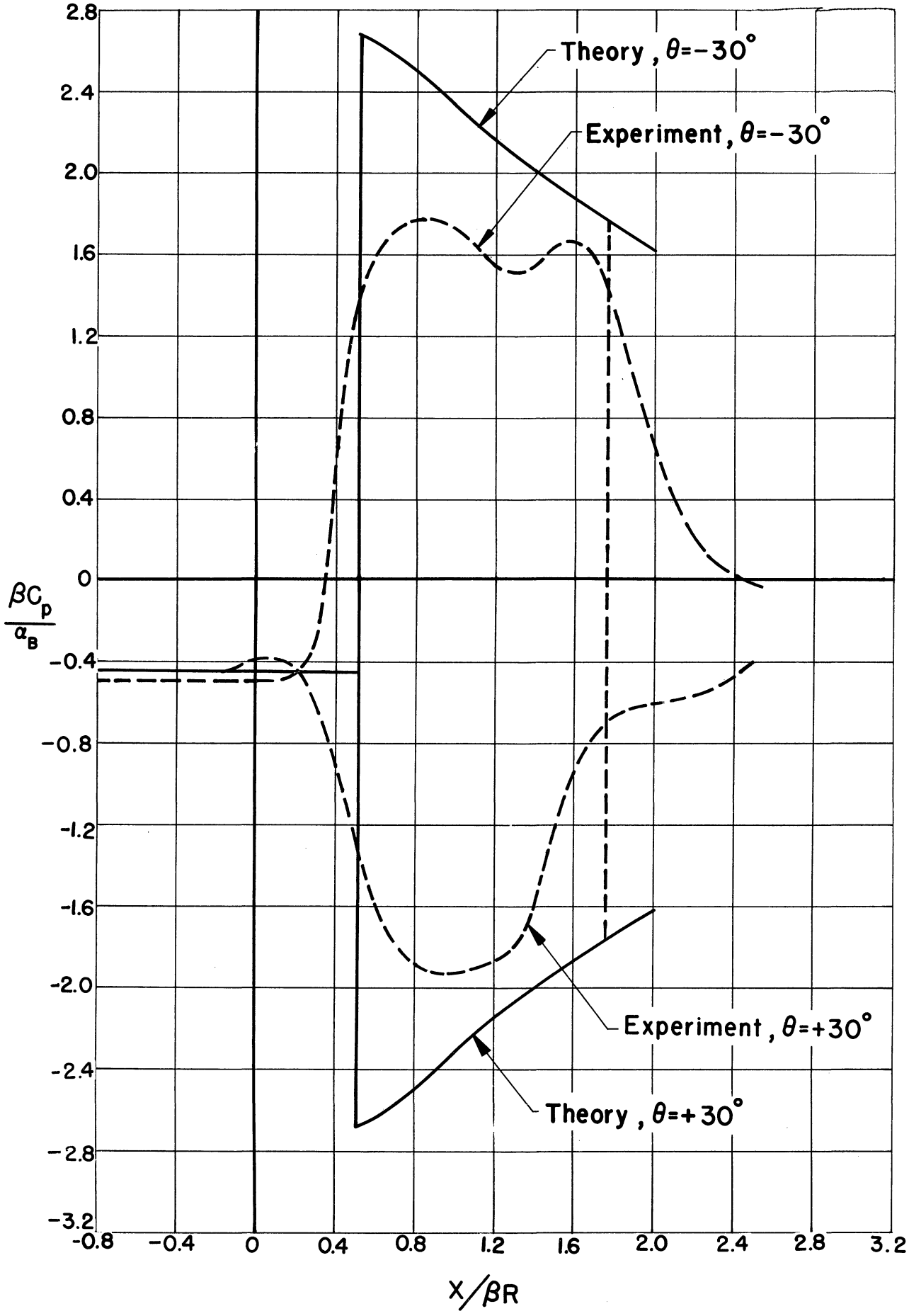

Fig. 22(Continued)

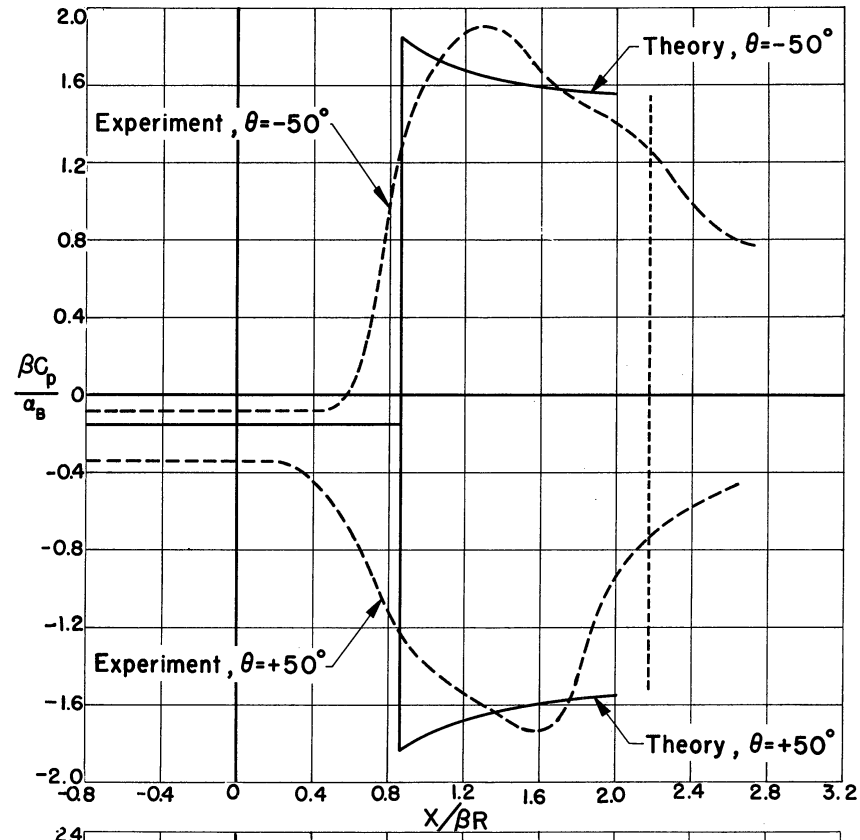

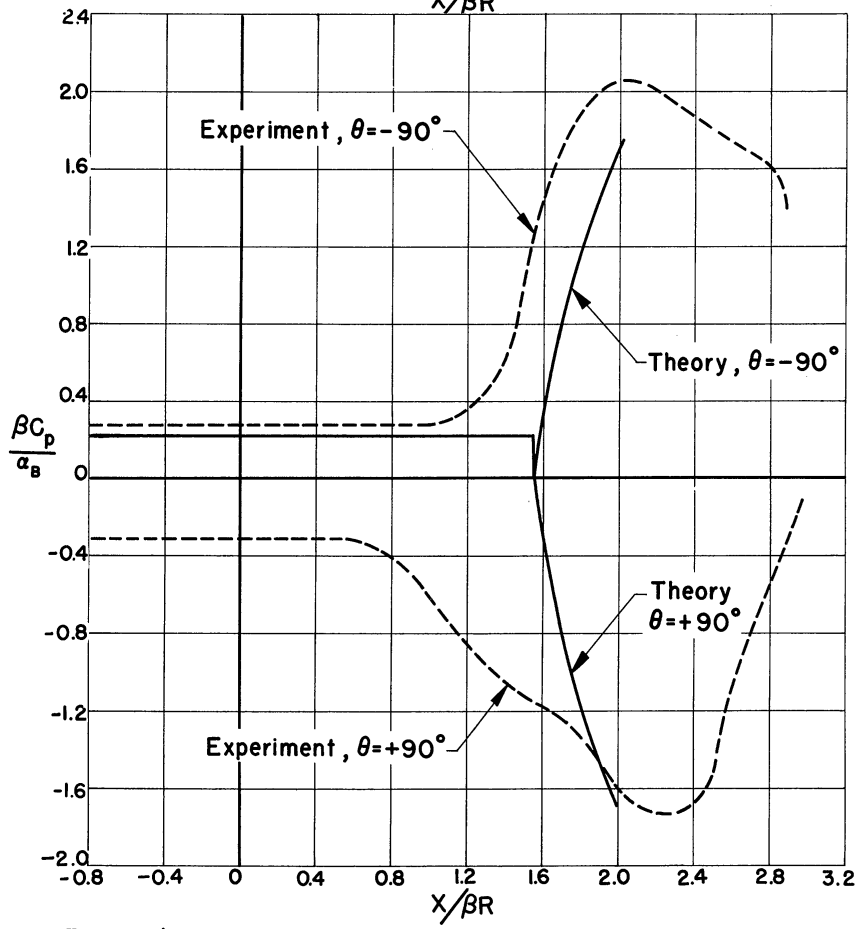

Fig. 22 (Concluded)

The same discussion as that in section D,7 with regard to the vertical shifting of the experimental pressure profiles applies to this configuration.

On the incident side of the body, the pressure profiles for $\theta = -10°$ show that there is a strong compression followed by a decrease in the axial pressure gradient, and then another sharp compression to the maximum pressure. The pressure profile for $\theta = -30°$ exhibits a sharp compression to the maximum pressure, followed by an expansion and a subsequent compression to a maximum value near the trailing edge. The appearance of this second compression in these two pressure profiles is accompanied by the same triangular band on the china-clay pattern as that mentioned in section D,3. Thus, it appears that the body boundary layer separates from the body and later reattaches farther downstream, in this case also to form a channel through which high-pressure air near the juncture of the wing leading edge and body flows radially out and back along the body surface. The pressure profiles for $\theta = -50$ and $-90°$ do not exhibit this characteristic double bump, so it is probable that the triangular-shaped separation region does not extend to these higher values of the meridional angle, or its thickness-to-length ratio may be small enough so that there is no sharp effect on the pressure profiles for these two meridional planes. This statement is further supported by the china-clay pattern, which indicates that the second, or reattachment, trace becomes indistinct at the higher values of θ.

The overall effect of the boundary layer is to soften the sharp spikes of the theoretically predicted pressure profiles considerably. Except for this softening effect and the appearance of the separated channel, the theory and experiment agree quite well.

On the lee side of the body the pressure profiles in the planes $\theta = +10$ and $+30°$ indicate that a very weak compression wave precedes the expansion wave just as in the case of the body at zero angle of attack and the wing at positive angles of attack. For the higher values of θ the steepness of the pressure gradient is considerably less, probably due to the combined effects of the spreading out of the expansion wave as it progresses around the body and the increased ease with which the pressure disturbances may be propagated upstream in the separated region on the lee side of the body.

All the pressure profiles indicate a strong tendency to return to the crossflow doublet-pressure distribution aft of the wing trailing edge. This tendency is also present on the china-clay patterns observed on the body.

The flow on the wing seems to be quite uniform on the body incident side, with perhaps a slight tendency for flow of the body boundary layer onto the wing surface. On the other hand, the china-clay pattern observed on the wing surface on the lee side of the body indicates that strong disturbances originate at both the outboard wing tip and the juncture between the body and

and the wing leading edge. The pattern is qualitatively quite similar to that in Fig. 8, with a separation over the rear portion of the wing surface which extends from near the body to about the half-span point and possibly even to the wing tip itself.

9. Body at Angle of Attack with Wing at Zero Angle of Attack, Wedge Surface of the Wing

On the lee side of the body the forward portion of the wedge surface of the wing is approximately aligned with the flow, so that only a relatively weak shock wave occurs at the wing leading edge. At the midchord position of the wing a strong expansion occurs, as is evident from the china-clay pattern observed on the body. At the wing trailing edge a strong shock occurs which deflects the flow back to approximately its original direction. This shock apparently separates the flow over the aft portion of the wing, as confirmed by the china-clay pattern on the wing, which shows that although the flow is deflected through the full 20° in passing the midchord point is separates approximately 3/4 inch forward of the wing trailing edge. Some flow from the forward half of the wing onto the body is also indicated by the china-clay pattern.

When the wedge surface of the wing is on the incident side of the body a strong shock wave is necessary to deflect the flow through 18° at the leading edge. The china-clay pattern shown in Fig. 23 indicates that there are two lines on the body, the first of which marks the local separation of the body boundary layer and the second of which marks the reattachment of the body boundary layer. Between the two lines the helical flow of the body boundary layer to higher values of θ is clearly visible.

The china-clay pattern on the wing shows that the flow expands through the full 20° at the midchord point and remains attached to the wing surface to within 1/4 inch of the wing trailing edge, after which it separates due to the shock at the wing trailing edge.

10. Body and Wing at Angle of Attack, Wedge Surface of the Wing

On the lee side of the body the china-clay pattern on the body shows that a slight expansion occurs at the wing leading edge. For values of $\theta < 30°$ it is apparent from the china-clay patterns on both the wing and the body that the flow separates at the midchord point; however, for the larger values of θ the flow on the body does curve downward toward the wing plane.

When the cambered side of the wing is on the incident side of the body the shock wave at the wing leading edge is very strong. Again, as in the case

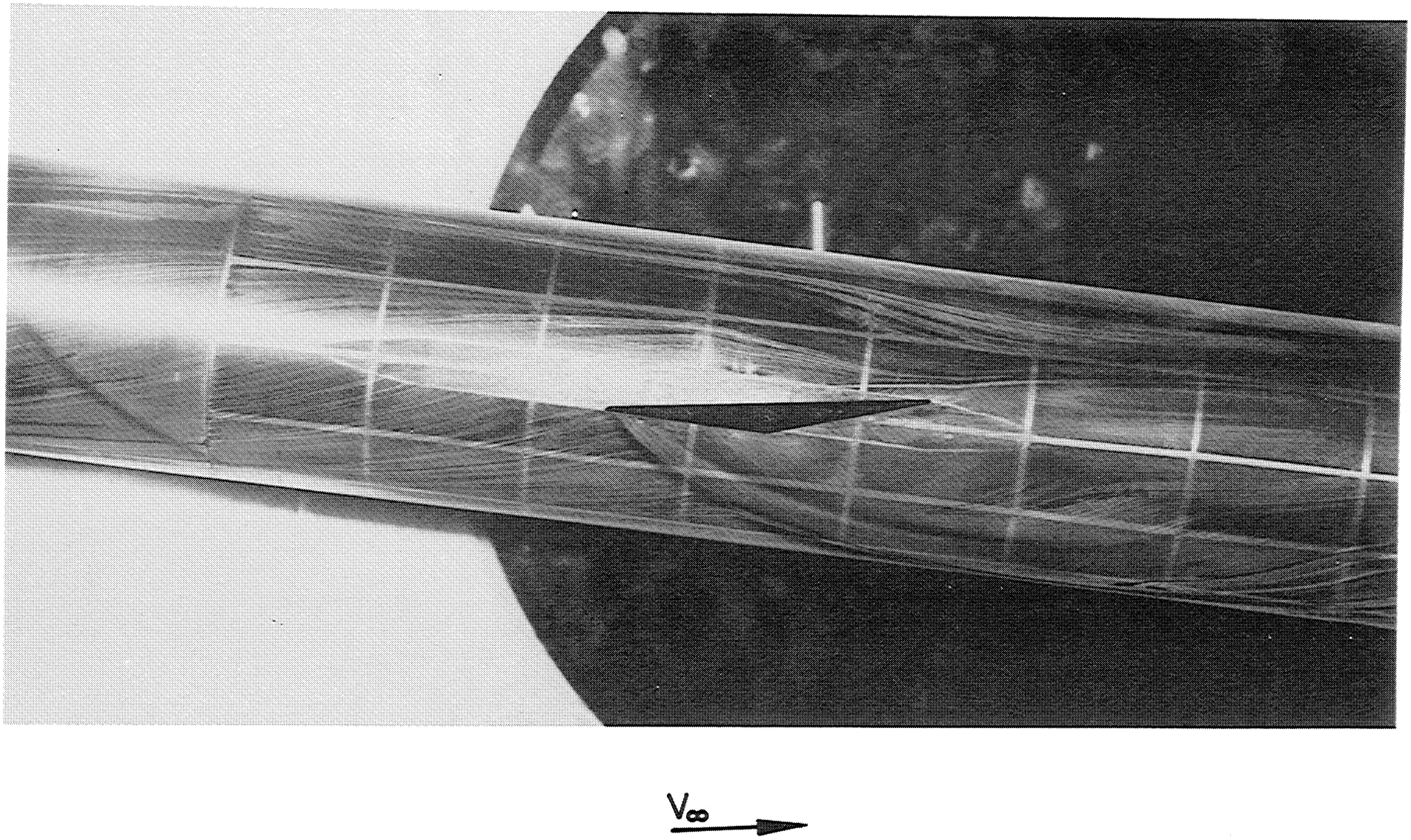

Fig. 23. China clay photograph: $\alpha_B = +8^\circ, \alpha_W = 0^\circ$, wedge surface side of wing down.

of the flat surface of the wing and body at 8° angle of attack as well as the body at zero angle of attack with wedge surface of the wing at +8° angle of attack, a triangular region with one vertex at the juncture of the wing leading edge and the body, which forms a separated channel for the boundary-layer crossflow, is visible in the china-clay pattern. For this configuration a composite of the experimental pressure profiles for several values of θ is shown in Fig. 24. The small bumps which are present in the profiles for θ = -10 and -30° are associated with the "separation bubble" previously mentioned.

The china-clay pattern observed on the wing indicates that there is no separation even over the rear portion of the wedge surface wing.

E. CONCLUSIONS

The experimental results obtained agree quite well with the values predicted by linearized theory as long as only those portions of the body upstream of the Mach helix from the juncture of the body and the wing trailing edge are considered. Beyond the trailing edge the theory is no longer valid and only the experimental results are applicable.

The agreement between theory and experiment can be improved by shifting the axial position at which the shock jumps are predicted by linearized theory to the position which is indicated by simple shock-wave theory (Fig. 5).

The presence of a viscous boundary layer on the body permits the forward propagation along the body of pressure disturbances generated at the wing leading edge. In addition, the wing leading-edge shock causes a strong crossflow of the body boundary layer which distorts the effective shape of the body. This distortion, in turn, causes a variable amount of forward propagation of pressure disturbances. For the case of a compressive shock at the wing leading edge the boundary-layer crossflow strongly resembles that reported in reference 11 on the lee side of a cylinder intersecting a plane shock wave.

Downstream of the wing trailing edge the measured pressure distributions together with the china-clay patterns observed on the body indicate a tendency for the flow to return to the free-stream conditions which prevail ahead of the wing leading edge.

The experimental results also indicate that a decrease in thickness of the turbulent boundary layer on the body causes a slight decrease in the viscous effects near the wing leading edge, and consequently better agreement between experiment and theory. On the other hand, the evidence of china-clay patterns

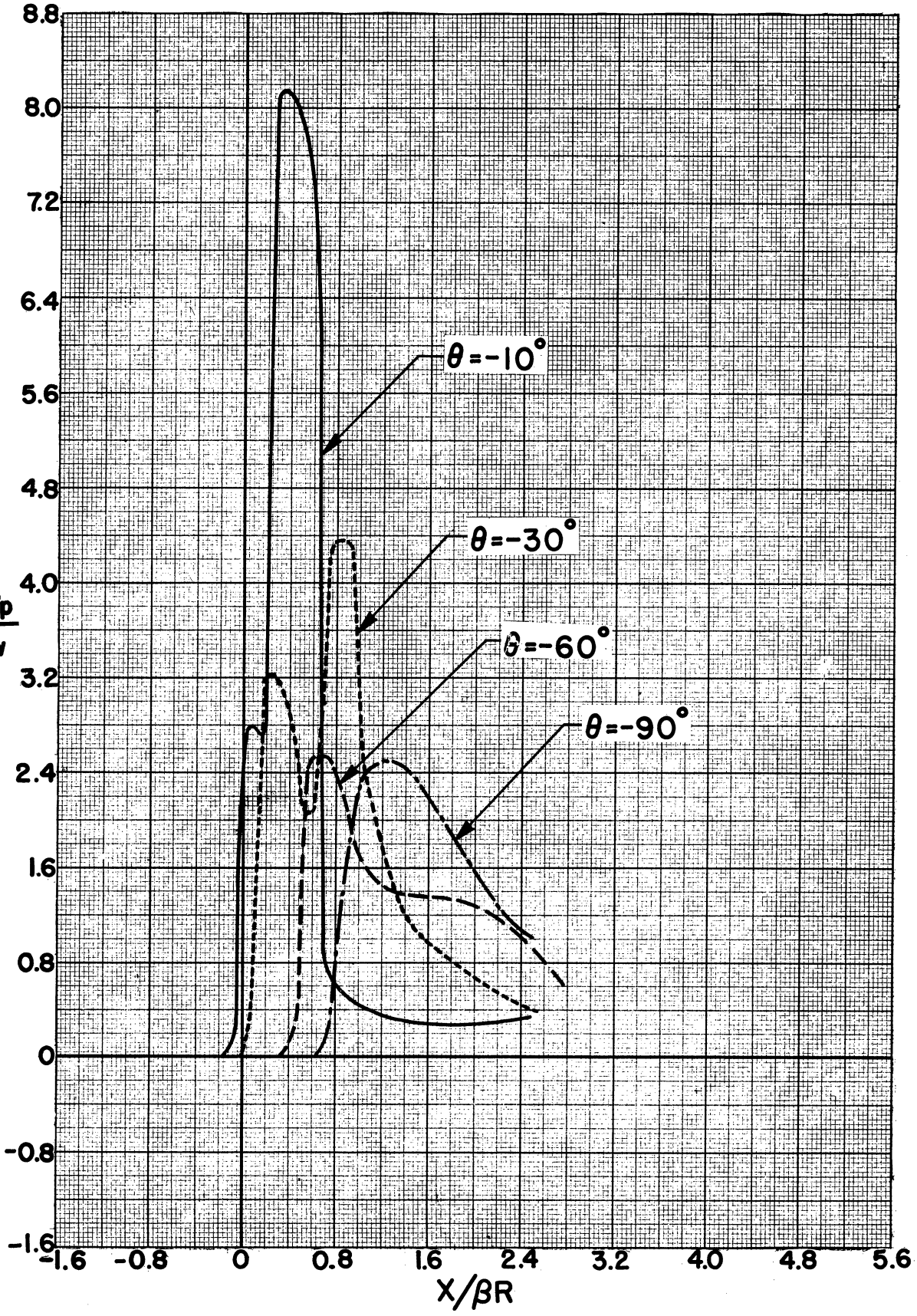

Fig. 24. Composite pressure profiles: $\alpha_B = +8^\circ, \alpha_W = +8^\circ$, wedge surface of the wing.

on the body indicates that the presence of a laminar boundary layer on the body will result in considerably increased upstream propagation of the disturbances generated at the wing leading edge. In this case it is possible that the pressure distributions observed on the body will differ from those predicted by linear theory. Thus the character of the body boundary layer, i.e., whether it is laminar or turbulent, may well exert a strong influence on the shape of the body pressure profiles.

The presence of extremely strong disturbances at the wing leading edge causes even the thicker turbulent boundary layer to separate locally from the body.

When the body is at an angle of attack the separation on the lee side, similar to that of reference 14, leads to poor agreement between theory and experiment. In addition, the separation of the laminar boundary layer on the wedge surface of the wing, which generally occurs near the midchord point, and the separation on the flat surface of the wing at the wing trailing edge due to the trailing edge shock wave increase the discrepancy between theory and experiment. It might well be that a turbulent boundary layer on the wing would suppress this separation and result in somewhat better agreement between theory and experiment.

The effect of a gap between wing and body appears to be small on such integrated quantities as total lift and total drag on the body, although the pressure profiles on the body in the vicinity of the gap are radically altered due to the presence of wing tip vortices at the inboard edge of the wing. The effect of the gap on the wing pressures is unknown, but it may be large enough so that the overall lift and drag of the body and wing in combination may be appreciably changed.

BIBLIOGRAPHY

1. Nielsen, J. N., "Supersonic Wing Body Interference," Ph.D. Thesis, California Institute of Technology, 1951.

2. Bardsley, O., "The Conditions at a Sharp Leading Edge in Supersonic Flow," Phil. Mag., 42, No. 326 (March, 1951).

3. Ferri, A., Elements of Aerodynamics of Supersonic Flows, The Macmillan Company, New York, 1949.

4. Liepmann, H. W., Roshko, A., and Dhawan, S., "On the Reflection of Shock Waves from Boundary Layers" N.A.C.A. TN 2334, April, 1951.

5. Shapiro, A. H., Neumann, E. P., and Barry, F. W., "Some Experiments on the Interaction of Shock Waves with Boundary Layers on a Flat Plate", Journal of Applied Mechanics, 17, No. 2 (June, 1950).

6. Bardsley, O., and Mair, W. A., "The Interaction between an Oblique Shock-Wave and a Turbulent Boundary Layer," Phil. Mag. 42, No. 324 (January, 1951).

7. Lees, L., "Interaction between the Laminar Boundary Layer over a Plane Surface and an Incident Oblique Shock Wave," Report No. 143, Princeton University, Aeronautical Engineering Laboratory, January, 1949.

8. Lighthill, M. J., "Reflection at a Laminar Boundary Layer of a Weak Steady Disturbance to a Supersonic Stream Neglecting Viscosity and Heat Conduction," Quarterly Journal of Mechanics and Applied Mathematics, 2, Part 3 (September, 1950).

9. Migotsky, E., and Morkovin, M. V., "Three Dimensional Shock Wave Reflections," Journal of the Aeronautical Sciences, 18, No. 7 (July, 1951).

10. Migotsky, E., "On the Reflection of Shock Waves in Three Dimensions," Ph.D. Thesis, University of Michigan, April, 1951.

11. Morkovin, M. V., Migotsky, E., Bailey, H. E., and Phinney, R. E., "Experiments on Interaction of Shock Waves and Cylinderical Bodies at Supersonic Speeds," Journal of the Aeronautical Sciences, 19, No. 4 (April, 1952).

12. Garby, L. C., and Nelson, W. C., "University of Michigan 8 x 13 Inch Intermittent-Flow Supersonic Wing Tunnel," University of Michigan Memorandum No. 59, Engineering Research Institute, June, 1950.

13. Murphy, J. S., and Phinney, R. E., "Viscoalization of Boundary Layer Flow," Readers' Forum, Journal of the Aeronautical Sciences, 18, No. 11 (November, 1951).

14. Allen, H. J., and Perkins, E. W., "A Study of Effects of Viscosity on Flow over Slender Inclined Bodies of Revolution," N.A.C.A. TR 1048, 1951.

15. Kuethe, A. M., and Schetzer, J. D., Foundations of Aerodynamics, John Wiley and Sons, New York, 1950.

16. Bailey, H. E., and Phinney, R. E., Final Report, Wing-Body Interference, Part I, Theoretical Investigation, University of Michigan, Engineering Research Institute, Project M937-1-F.